Journal of Inflammation Research

Dovepress
Taylor & Francis Group

Open Access Full Text Article

ORIGINAL RESEARCH

Mechanisms of Yiqi Huoxue Granule in Atherosclerosis Treatment: Insights from UPLC-Q-Exactive Orbitrap-MS Analysis, Network Pharmacology, Molecular Docking, and Experimental Verification

Xinzhou Wang[1,*], Shanshan Liu[1,*], Zehao Lei[2], Panxia Cao[2], Weili Shi[1], Shuibo Gao[1], Hong Wu[1,3]

[1]Second Clinical Medical College, Henan University of Chinese Medicine, Zhengzhou, 450002, People's Republic of China; [2]Graduate School, Henan University of Chinese Medicine, Zhengzhou, 450046, People's Republic of China; [3]Institute of Cardiovascular Disease, Henan University of Chinese Medicine, Zhengzhou, 450002, People's Republic of China

*These authors contributed equally to this work

Correspondence: Hong Wu, Email wuhong@hactcm.edu.cn

Background: Yiqi Huoxue Granule (YQHX), a traditional Chinese medicine (TCM) formulation, is extensively utilized for the treatment of atherosclerotic diseases. However, its active constituents and molecular mechanisms remain unclear. We utilized a systematic methodology to identify bioavailable compounds in vivo and predict and validate the principal targets and pathways responsible for their anti-atherosclerotic actions.

Methods: Serum pharmacochemistry utilizing UPLC-Q-Exactive Orbitrap-MS was employed to identify the bioavailable compounds of YQHX. An integrated methodology combining network pharmacology and molecular docking was implemented to predict its potential targets and mechanisms against atherosclerosis, which were subsequently verified experimentally in apolipoprotein E-deficient ($ApoE^{-/-}$) mice.

Results: We identified 36 absorbable compounds in the serum of rats following YQHX administration, and 252 potential therapeutic targets were predicted. Protein-protein interaction analysis identified 10 hub targets, which are IL-6, TNF, EGFR, TP53, AKT, STAT3, SRC, CTNNB1, TLR4, and MMP-9. Enrichment analyses indicated that these targets are primarily involved in lipid metabolism and inflammatory responses, with significant enrichment in the PI3K-Akt and SRC signaling pathways. Molecular docking revealed strong binding affinities between the proteins EGFR, SRC, and AKT and their respective compounds. In $ApoE^{-/-}$ mice, YQHX significantly attenuated atherosclerotic plaque progression, enhanced lipid profiles, and inhibited systemic and plaque inflammation (decreased IL-6, IL-1β, sVCAM-1, and macrophage infiltration). Western blotting analysis revealed that these benefits were associated with the inhibition of SRC and AKT phosphorylation within the plaques.

Conclusion: This study systematically identified the bioactive compounds of YQHX and demonstrated its multi-target anti-atherosclerotic effect, which involved the enhancement of lipid metabolism and suppression of inflammation, mediated, at least in part, by the inhibition of the SRC/AKT signaling pathway.

Keywords: Yiqi Huoxue granule, atherosclerosis, UPLC-Q-Exactive Orbitrap-MS, network pharmacology, inflammation

Introduction

Atherosclerosis (AS), a critical precursor to major cardiovascular and cerebrovascular diseases, including coronary heart disease and stroke, remains a severe global health issue.[1,2] Despite advancements in the understanding of AS, which has markedly enhanced its diagnosis and treatment, it remains the leading cause of death worldwide.[3] Therapies targeting blood lipid regulation and blood pressure management have demonstrated efficacy in decelerating plaque progression and

https://doi.org/10.2147/JIR.S566368
Received: 18 September 2025
Accepted: 5 January 2026
Published: 24 January 2026

diminishing cardiovascular events. The high prevalence of acute cardiovascular events highlights the urgent need for sustained research and innovation in this field.

In recent decades, AS has gained more attention as a chronic inflammatory disease.[4,5] The formation of atherosclerotic plaques is primarily a pathophysiological process influenced by the interaction between lipid metabolism dysregulation and chronic inflammation.[6,7] Oxidized low-density lipoprotein (ox-LDL) stimulates endothelial cells to produce adhesion molecules, facilitating the infiltration of monocytes that subsequently differentiate into macrophages.[8] These macrophages engulf ox-LDL through scavenger receptors, resulting in foam cell formation, and simultaneously secrete pro-inflammatory cytokines, thus sustaining a self-amplifying inflammatory cycle.[9] Matrix metalloproteinases (MMPs) within the inflammatory microenvironment degrade extracellular matrix components of the fibrous cap, hence enhancing plaque susceptibility.[10] Collectively, these findings underscore inflammation as a crucial connection between lipid deposition and plaque rupture, offering a robust mechanistic rationale for anti-inflammatory therapeutic strategies targeting AS.

In traditional Chinese medicine (TCM), AS is primarily attributed to "Qi deficiency," which disrupts circulation and culminates in "blood stasis," a pattern commonly observed in patients with AS.[11] Yiqi Huoxue Granule (YQHX)—composed of *Astragali Radix, Ginseng Radix et Rhizoma, Paeoniae Rubra Radix*, and *Carthami Flos*—derives from the therapeutic principles of "Qi-tonifying" and "blood-activating." Astragali Radix and Ginseng Radix et Rhizoma act as the "Jun Yao," enhancing Qi and facilitating hemodynamics, whereas Paeoniae Rubra Radix and Carthami Flos stimulate circulation and alleviate stasis. Conceptually, "Qi" correlates with cellular energy metabolism and immune homeostasis, whereas "blood stasis" corresponds to endothelial dysfunction, compromised microcirculation, and hemorheological abnormalities. Therefore, the TCM strategy of "invigorating Qi and activating blood" may mechanistically correspond to restoring bioenergetic capacity, enhancing endothelial function, and modulating vascular inflammation—processes pivotal to AS initiation and progression.

Our previous study has demonstrated that, across in vitro lipopolysaccharide (LPS)-induced endothelial cell and in vivo LPS-challenged mouse models, YQHX mitigated endothelial inflammation by reducing tumor necrosis factor-alpha (TNF-α), interleukin-6 (IL-6), and IL-8, and down-regulating vascular cell adhesion molecule-1 (VCAM-1) and intercellular adhesion molecule-1—thereby reducing endothelial injury and promoting an anti-inflammatory, endothelium-protective profile pertinent to atherogenesis.[12,13] However, the active constituents and the precise mechanisms underlying YQHX's effects on AS require more clarification. A primary issue in investigating complex TCM formulae is that they comprise hundreds of constituents, yet only a fraction is absorbed into the bloodstream and potentially exerts systemic effects. Serum pharmacochemistry aims to detect bioavailable compounds in the bloodstream post-administration, thereby enriching for the most likely active components.[14] High-resolution platforms such as ultra-performance liquid chromatography–quadrupole-Exactive Orbitrap–mass spectrometry (UPLC-Q-Exactive Orbitrap-MS) provide sensitive detection and characterization of these exposure-driven candidates.[15] Given the multi-component, multi-target nature of YQHX, computational approaches capable of integrating chemical, genetic, and pathway-level information are essential to systematically identify its potential mechanisms of action. Network pharmacology, which integrates high-throughput data analysis and multidimensional pharmacological information, can elucidate the complex interactions among compounds, targets, and diseases.[16]

Therefore, to comprehensively elucidate the mechanisms of action of YQHX, we employed an integrated strategy that combined UPLC-Q-Exactive Orbitrap-MS to identify and characterize active components, network pharmacology to hypothesize their putative synergistic targets and pathways, molecular docking to evaluate key interactions, and, finally, in vivo studies using apolipoprotein E knockout ($ApoE^{-/-}$) mice to functionally validate the predicted anti-atherosclerotic effects. We selected $ApoE^{-/-}$ mice because they develop human-like, lipid-rich, inflamed atherosclerotic plaques, particularly on a high-fat diet, and are widely recognized as a gold-standard model for assessing anti-atherosclerotic interventions due to their robust, reproducible lesion formation and well-defined pathophysiology.[17]

Materials and Methods

Preparation of YQHX

YQHX was acquired from Neo-Green Pharmaceutical Technology Development Co., Ltd. (Chengdu, China). YQHX comprised four traditional Chinese herbal medicine extracts (particles), *Astragali Radix* (Batch No. 17,100,048), *Ginseng Radix* et Rhizoma (Batch No. 17,020,134), *Paeoniae Rubra Radix* (Batch No. 17,080,143), and *Carthami Flos* (Batch No. 17,060,133), which were

mixed in a ratio of 3:3:2:1. Table 1 illustrates the dry weight of each of the raw ingredients per 8 g of YQHX. The authenticity of each extract was validated utilizing high-performance liquid chromatography, as in a previous study.[18] For experimental use, 5 g of YQHX was dissolved in 10 mL of normal saline, followed by ultrasonic treatment to ensure complete dispersion.

Experimental Animals

Eight-week-old male Sprague-Dawley rats and six-week-old C57BL/6J ApoE$^{-/-}$ mice (specific pathogen-free grade) were procured from Spefor Biotechnology Co., Ltd (Beijing, China) under Certificate No. SCXK (Beijing) 2019–0010. These animals were housed at the Henan Province Hospital of Traditional Chinese Medicine's animal experimental center. All animal experiments were conducted following the ARRIVE guidelines (https://arriveguidelines.org/arrive-guidelines) and approved by the Medical Ethical Committee of Henan Province Hospital of Traditional Chinese Medicine (Zhengzhou, China, approval number: PZ-HNSZYY-2022-035).

Serum Sample Preparation for Absorbed Component Determination

After one week of adaptive feeding, the rats were randomly stratified into two groups based on a randomization table, with 10 rats in each group. The YQHX group received continuous administration of YQHX (2.16 g/kg/day) through oral gavage, whereas the control group received an equivalent volume of normal saline. One hour post-final gavage, rats were anesthetized with isoflurane (4% for induction; 1.5% for maintenance in oxygen at 1 L/min). The surgical plane of anesthesia was verified by the absence of pedal withdrawal and corneal reflexes. Blood was obtained through exsanguination via the abdominal aorta, and euthanasia was performed under deep anesthesia by bilateral thoracotomy to ensure death. No animals were permitted to recuperate after anesthesia. Whole blood was allowed to clot at room temperature for 30 min and subsequently centrifuged to obtain serum. A 100 μL aliquot of serum was mixed with four volumes of pre-chilled methanol and incubated in an ice bath for 1 h. After centrifugation at 16,000 g at 4 °C for 20 min, the supernatant was obtained and dried under nitrogen gas. The residue was subsequently reconstituted in pre-chilled 50% methanol and centrifuged at 20,000 g at 4 °C for 10 min. Eventually, 50 μL of the supernatant was collected for subsequent analysis.

UPLC-Q-Exactive Orbitrap-MS Analysis

Samples were analyzed using a Shimadzu LC-30 ultra-high-performance liquid chromatography (UHPLC) system equipped with an ACQUITY UPLC® HSS T3 column (2.1 × 100 mm, 1.8 μm; Cat. #186003539, Waters). Samples were kept at 4 °C in the autosampler throughout the analytical run. Chromatographic separation was carried out at 40 °C with a flow rate of 0.3 mL/min. The mobile phase consisted of solvent A (0.1% formic acid in water) and solvent B (0.1% formic acid in acetonitrile). The gradient elution program was as follows: 0–5 min, 0% B; 5–20 min, 0–100% B; 20–25 min, 100% B; 25–25.1 min, 100–0% B; and 25.1–30 min, 0% B. Following UHPLC separation, mass spectrometric detection was performed on a Q-Exactive Plus Orbitrap mass spectrometer (Thermo Scientific) equipped with a heated electrospray ionization source. Data were acquired in both positive and negative ion modes under the following ionization parameters: spray voltage, 3.8 kV (positive) and 3.2 kV (negative); capillary temperature, 320 °C; sheath gas, 30 arbitrary units; auxiliary gas, 5 arbitrary units; probe heater temperature, 350 °C; and S-lens RF level, 50. Full MS

Table 1 Four Raw Ingredients of YQHX

Chinese Name	Drug Name	Scientific Name[a]	Family	Quantity (Dry, g)
Huangqi	Astragali Radix	*Astragalus membranaceus* Bunge	Fabaceae	30
Renshen	Ginseng Radix et Rhizoma	*Carthamus tinctorius* L. (Carthami Flos), *Panax ginseng* C. A. Mey.	Araliaceae	15
Chishao	Paeoniae Rubra Radix	*Paeonia anomala subsp. veitchii* (Lynch) D.Y.Hong & K.Y.Pan	Ranunculaceae	15
Honghua	Carthami Flos	*Carthamus tinctorius* L.	Asteraceae	10

Notes: [a]The Latin name of the plants was verified using the World Flora Online database (http://www.worldfloraonline.org/).

scans were acquired over an m/z range of 90–1350 at a resolution of 70,000 (m/z 200), with an automatic gain control (AGC) target of 3×10^6 and a maximum injection time of 100 ms. Data-dependent MS/MS acquisition (Top10 mode) was employed, in which the ten most intense precursor ions in each full scan were fragmented by higher-energy collisional dissociation. MS/MS spectra were acquired at a resolution of 17,500 (m/z 200), with an AGC target of 1×10^5, a maximum injection time of 50 ms, an isolation window of 2.0 m/z, and stepped normalized collision energies of 20, 30, and 40. The total acquisition time per sample was 30 min. Raw LC-MS/MS data were processed using MS-DIAL software (version 4.80) for peak detection, alignment, retention time correction, and peak area integration. Metabolite identification was performed based on accurate mass and MS/MS fragmentation pattern matching, with mass tolerances set to <0.01 Da for full MS and <0.02 Da for MS/MS.

Analysis of Network Pharmacology

Potential targets of each absorbed compound were predicted utilizing the Swiss Target Prediction database.[19] The term "Atherosclerosis" enabled the identification of disease-related targets across databases, including GeneCards,[20] DrugBank,[21] OMIM,[22] and PharmGkb[23] databases. Intersection targets were analyzed utilizing Venny software (version 2.1). Protein-protein interaction (PPI) analysis employed a minimum interaction threshold of > 0.7 using the STRING database,[24] with results exported for subsequent examination. Enrichment analyses for Gene ontology (GO) and Kyoto encyclopedia of genes and genomes (KEGG) were conducted using the DAVID database.[25] Network visualization and analysis were performed using Cytoscape software (version 3.7.2).[26]

Molecular Docking

Molecular docking was performed utilizing AutoDock Vina (version 1.2.2)[27] to evaluate the binding affinities and interaction modalities between candidate compounds and target proteins. The three-dimensional (3D) coordinates of target proteins and the chemical structures of the compounds were acquired from the Protein Data Bank[28] and PubChem,[29] respectively. All files were converted into PDBQT format, with water molecules omitted and polar hydrogen atoms incorporated, with a binding affinity threshold of ≤ –5.0 kcal/mol, signifying strong interactions.

Animal Model Establishment and Drug Administration

After a two-week acclimatization period, C57BL/6J ApoE$^{-/-}$ mice were randomly allocated to five groups (n = 10 per group) using a randomization table: control, model, high-dose YQHX (YQHX-H), low-dose YQHX (YQHX-L), and rosuvastatin (RST). All groups, except the control group, which was maintained on a standard chow diet, were fed a high-fat diet (HFD) for 16 weeks to induce atherosclerosis. Pharmacological interventions were commenced two weeks after the initiation of HFD feeding. The high-dose and low-dose YQHX groups received YQHX at 2.8 g/kg/day and 1.4 g/kg/day, respectively, through oral gavage, whereas the RST group received rosuvastatin at 2.08 mg/kg/day. All treatments were administered daily for 14 weeks. The mice were euthanized at the end of the 16-week modeling period. At the end of the study, terminal procedures were performed under deep isoflurane anesthesia (4% for induction; 1.5% for maintenance in oxygen at 1 L/min), with a surgical plane of anesthesia verified by the absence of pedal withdrawal and corneal reflexes. Blood was obtained through exsanguination via cardiac puncture, and euthanasia was performed under deep anesthesia by bilateral thoracotomy to confirm death. No animals were allowed to recuperate from anesthesia. Samples of the aorta and liver were collected for pathological and molecular analyses. The serum was subsequently separated to analyze inflammatory markers and lipid profiles. Heart, liver, and aortic tissues were immersed in 4% polyformaldehyde or snap-frozen for pathological staining or molecular biological analysis.

Histopathological Staining

The hematoxylin-eosin (HE) (Cat. #G1120, Solarbio) and Oil Red O (ORO) (Cat. #G1261, Solarbio) staining of frozen sections from mouse heart and liver tissues, along with en face ORO staining (Cat. #G1260, Solarbio) of the aorta, were executed in full adherence to the kit's instructions. Imaging was captured utilizing an optical microscope (Eclipse 80i, Nikon).

Immunohistochemistry Staining

Immunohistochemistry (IHC) staining (Cat. #PK10006, Proteintech) was performed following the manufacturer's instructions. After dehydration and antigen retrieval, paraffin-embedded tissue sections were incubated with blocking buffer at 37 °C for 30 min. The sections were subsequently incubated overnight at 4 °C with anti-F4/80 antibody (1:5000, Cat. #29414-1-AP, Proteintech). After extensive washing, the sections were treated with a horseradish peroxidase (HRP)-conjugated secondary antibody for 30 min at room temperature. Subsequently, the DAB color-developing solution was added dropwise. The sections were subsequently counterstained with hematoxylin, and images were acquired.

Enzyme-Linked Immunosorbent Assay (ELISA)

According to the manufacturer's protocols for TNF-α (Cat. #EK282, Lianke), IL-6 (Cat. #EK206, Lianke), interleukin-1 beta (IL-1β; Cat. #EK201B, Lianke), and soluble VCAM-1 (sVCAM-1) (Cat. #EK290, Lianke) ELISA kits, mouse serum samples were introduced into microplate wells and incubated with a diluted primary antibody solution. After washing, the wells were incubated with a diluted secondary antibody solution and developed with substrate solution for 5–10 min. The reaction was terminated utilizing a stop buffer, and absorbance was measured at 450 nm to determine protein concentrations.

Western Blotting

After mixing with loading buffer, protein samples were separated by sodium dodecyl sulfate–polyacrylamide gel electrophoresis and transferred onto a polyvinylidene fluoride membrane (Cat. #IPVH00010, Millipore). The membrane was incubated with primary antibodies targeting p-SRC (1:1000, Cat. #80706-2-RR, Proteintech), SRC (1:1000, Cat. #60315-1-Ig, Proteintech), p-AKT (1:1000, Cat. #66444-1-Ig, Proteintech), AKT (1:1000, Cat. #10176-2-AP, Proteintech), followed by incubation with suitable secondary antibodies. After washing, membranes were subjected to enhanced chemiluminescent solution (Cat. #PK10001, Proteintech) for 3 min. Images were obtained using a chemiluminescent imaging system (ChemiDoc XRS+, Bio-Rad), and band intensities were measured using ImageJ software.

Statistics Analysis

Data were analyzed utilizing IBM Statistical Package for the Social Sciences software Statistics (Version 19.0) and are presented as mean ± standard deviation (SD). The Shapiro–Wilk and Levene's tests were utilized to verify assumptions of normality and homogeneity of variances, respectively. An independent *t*-test was utilized for normal data, whereas the Mann–Whitney *U*-test was employed for non-normal data in two-group comparisons. For multiple-group comparisons, one-way analysis of variance (ANOVA) with Tukey's post-hoc test was utilized for parametric data; Welch's ANOVA with Dunnett's T3 test was employed for data with unequal variances; and the Kruskal–Wallis test with Dunn's test was employed for non-parametric data. Statistical significance was set at $P < 0.05$, and exact *P*-values are reported.

Results

Determination of Components in YQHX

UPLC-Q-Exactive Orbitrap-MS was utilized for qualitative identification of the absorbable constituents of YQHX. We identified 36 absorbable compounds across positive and negative ion modes. Representative base peak chromatograms and detailed compound characterizations are presented in Figure 1 and Table 2, respectively, and the non-absorbed constituents detected in the formula are listed in Supplemental Table S1.Among these absorbed compounds, prenol lipids (n = 11) represented the predominant class, potentially serving as the principal bioactive constituents responsible for the anti-atherosclerotic effects of YQHX. These findings establish a foundation for further investigation of the therapeutic mechanisms of YQHX and the development of novel anti-atherosclerotic agents.

Construction of the PPI Network

Supplementary Figure S1 depicts the analytical workflow for network pharmacology analysis. Based on database predictions, 861 targets were identified for the 36 absorbed compounds. Querying databases with the keyword "atherosclerosis" yielded 1,524 associated targets. Consequently, 252 overlapping therapeutic targets were identified (Figure 2A). In the PPI network

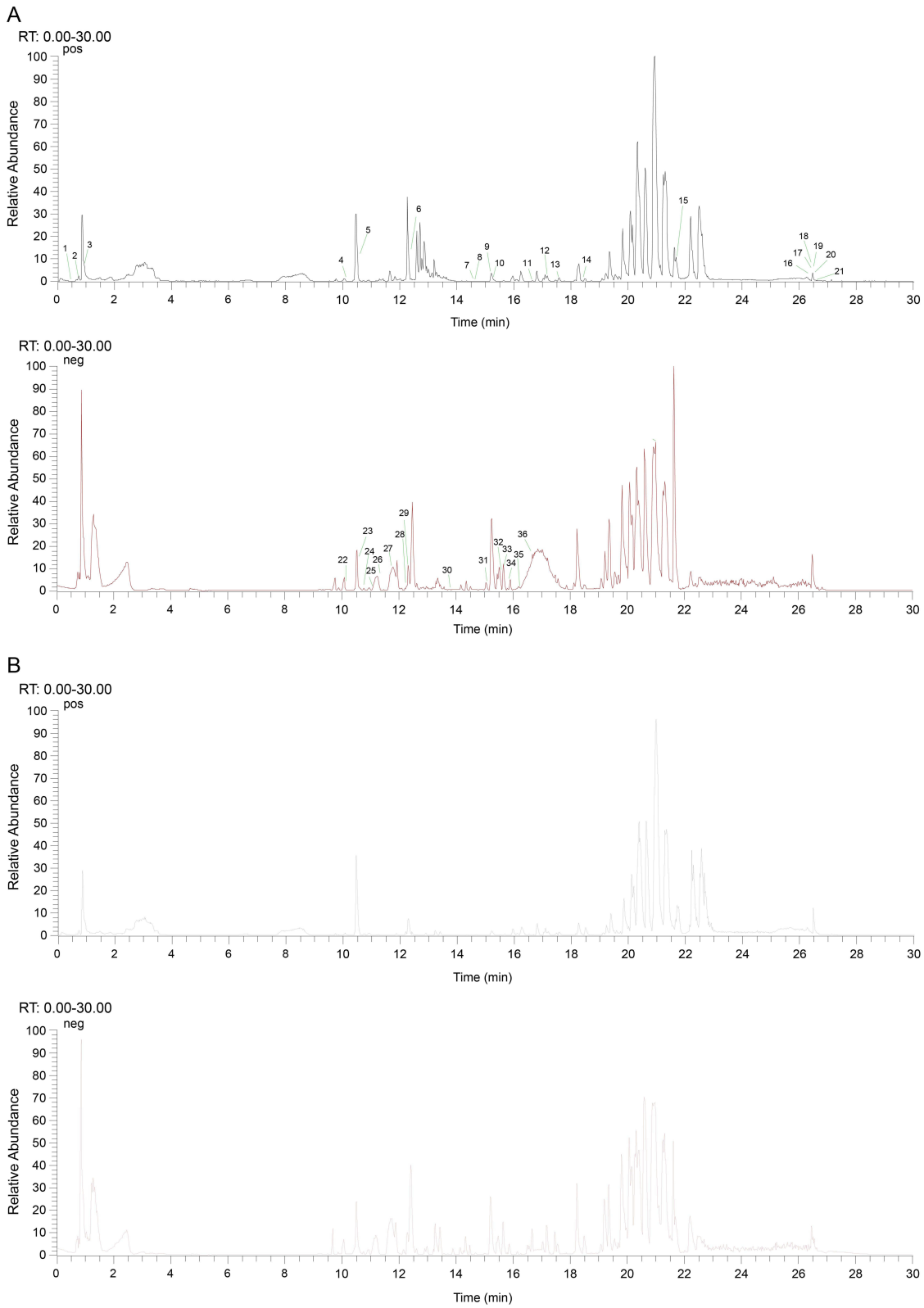

Figure 1 Typical base peak chromatograms of the 36 absorbed compounds detected by UPLC-Q-Exactive Orbitrap-MS. (**A**) Base peak chromatograms of serum containing YQHX in positive and negative ion modes. (**B**) Base peak chromatograms of blank serum in positive and negative ion modes.

Table 2 Detailed Characterizations of 36 Absorbed Compounds

No.	Compounds	Ion Mode	Formula	PPM	RT (min)	Cal. m/z	Class	Identification Source
YQHX1	Camphene	[M+H]+	$C_{10}H_{16}$	1.53137	0.508	137.13269	Prenol lipids	KEGG, HMDB
YQHX2	Galactosamine	[M+Na]+	$C_6H_{13}NO_5$	1.33618	0.812	202.06889	Organooxygen compounds	KEGG, PubChem, HMDB
YQHX3	Furanodienone	[M+H]+	$C_{15}H_{18}O_2$	3.82485	0.922	231.13387	Prenol lipids	KEGG, HMDB
YQHX4	Kojic acid	[M+H]+	$C_6H_6O_4$	0.69914	10.337	143.03397	Pyrans	KEGG, PubChem, HMDB
YQHX5	Maltol	[M+H]+	$C_6H_6O_3$	1.88918	10.544	127.03922	Pyrans	KEGG, PubChem, HMDB
YQHX6	Albiflorin	[M+H]+	$C_{23}H_{28}O_{11}$	1.64183	12.419	481.16959	Prenol lipids	KEGG, PubChem, HMDB
YQHX7	Diosmetin 7-O-beta-D-glucuronopyranoside	[M+H]+	$C_{22}H_{20}O_{12}$	3.12302	14.505	477.10129	Flavonoids	PubChem, HMDB
YQHX8	4H-1-Benzoicpyran-4-one, 5-hydroxy-2-(4-hydroxyphenyl)	[M+H]+	$C_{15}H_{10}O_4$	1.88187	14.622	255.06471	Flavonoids	PubChem
YQHX9	3-Phenyllactic acid	[M+H]+	$C_9H_{10}O_3$	0.11971	15.167	167.0703	Phenylpropanoic acids	KEGG, PubChem, HMDB
YQHX10	3-(2-hydroxy-3,4-dimethoxyphenyl)-3,4-dihydro-2H-1-benzopyran-7-ol	[M+H]+	$C_{17}H_{18}O_5$	2.40827	15.213	303.12195	Isoflavonoids	PubChem, HMDB
YQHX11	Ginsenoside Rb1	[M+FA-H]-	$C_{54}H_{92}O_{23}$	0.84951	15.853	1153.60205	Prenol lipids	KEGG, PubChem, HMDB
YQHX12	Ginsenoside Rb2	[M+FA-H]-	$C_{53}H_{90}O_{22}$	1.62871	16.209	1123.58862	Prenol lipids	PubChem, HMDB
YQHX13	Dipterocarpol	[M+H]+	$C_{30}H_{50}O_2$	1.87195	16.689	443.38754	Prenol lipids	KEGG, PubChem
YQHX14	Soyasaponin I	[M+H]+	$C_{48}H_{78}O_{18}$	0.06359	17.316	943.526	Prenol lipids	KEGG, HMDB
YQHX15	Formononetin	[M+H]+	$C_{16}H_{12}O_4$	1.33789	17.543	269.08051	Isoflavonoids	KEGG, PubChem, HMDB
YQHX16	Oleanolic acid	[M+H-H2O]+	$C_{30}H_{48}O_3$	1.18355	18.366	439.35751	Prenol lipids	KEGG, PubChem, HMDB
YQHX17	Vitamin K2	[M+H]+	$C_{31}H_{40}O_2$	2.37758	21.598	445.31293	Prenol lipids	KEGG, PubChem, HMDB
YQHX18	PC(16:0/18:1)	[M+H]+	$C_{42}H_{82}NO_8P$	3.28694	26.46	760.58258	Glycerophospholipids	PubChem, HMDB
YQHX19	PC(18:1/18:2)	[M+H]+	$C_{44}H_{82}NO_8P$	1.47849	26.462	784.58624	Glycerophospholipids	PubChem, HMDB
YQHX20	PC(16:0/16:0)	[M+H]+	$C_{40}H_{80}NO_8P$	2.81798	26.463	734.57147	Glycerophospholipids	PubChem, HMDB
YQHX21	PC(18:0/18:2)	[M+H]+	$C_{44}H_{84}NO_8P$	0.92804	26.464	786.60144	Glycerophospholipids	PubChem, HMDB
YQHX22	PC(O-18:1/20:4)	[M+H]+	$C_{46}H_{84}NO_7P$	0.39013	26.467	794.60608	Glycerophospholipids	HMDB
YQHX23	PC(18:0/20:4)	[M+H]+	$C_{46}H_{84}NO_8P$	2.40562	26.519	810.60266	Glycerophospholipids	PubChem, HMDB
YQHX24	Chlorogenic acid	[M-H]-	$C_{16}H_{18}O_9$	2.40733	10.172	353.08698	Organooxygen compounds	KEGG, PubChem, HMDB
YQHX25	Purine	[M-H]-	$C_5H_4N_4$	3.70644	10.586	119.03326	Imidazopyrimidines	KEGG, PubChem, HMDB
YQHX26	Citrazinic acid	[M-H]-	$C_6H_5NO_4$	3.84313	10.627	154.01295	Pyridines and derivatives	PubChem
YQHX27	Dihydromelilotoside	[M-H]-	$C_{15}H_{20}O_8$	1.49797	11.07	327.10803	Organooxygen compounds	PubChem, HMDB
YQHX28	Gentisic acid	[M-H]-	$C_7H_6O_4$	2.78295	11.387	153.01767	Benzene and substituted derivatives	KEGG, HMDB
YQHX29	Gallic acid methyl ester	[M-H]-	$C_8H_8O_5$	2.48512	11.681	183.02855	Benzene and substituted derivatives	PubChem, HMDB
YQHX30	Dihydroferulic acid	[M-H]-	$C_{10}H_{12}O_4$	3.07452	12.261	195.06493	Phenylpropanoic acids	PubChem, HMDB
YQHX31	Quercetin 3-Gentiobioside	[M-H]-	$C_{27}H_{30}O_{17}$	0.09598	12.399	625.14099	Flavonoids	PubChem, HMDB
YQHX32	Spiraeoside	[M-H]-	$C_{21}H_{20}O_{12}$	0.19361	13.739	463.08823	Flavonoids	HMDB
YQHX33	Calceolarioside A	[M-H]-	$C_{23}H_{26}O_{11}$	1.27845	15.168	477.13962	Cinnamic acids and derivatives	PubChem
YQHX34	Abscisic acid	[M-H]-	$C_{15}H_{20}O_4$	1.59618	15.547	263.12839	Prenol lipids	KEGG, HMDB
YQHX35	Ethyl vanillate	[M-H]-	$C_{10}H_{12}O_4$	1.79154	15.637	195.06822	Benzene and substituted derivatives	PubChem, HMDB
YQHX36	Ginsenoside Re	[M-H]-	$C_{48}H_{82}O_{18}$	3.23509	16.693	945.5379	Prenol lipids	KEGG, PubChem, HMDB

Notes: Compound identification was based on MS/MS spectral matching against public databases (KEGG, PubChem, HMDB) and an in-house mzVault library, using mass accuracy (< 5 ppm) and characteristic fragment ions as the primary criteria.

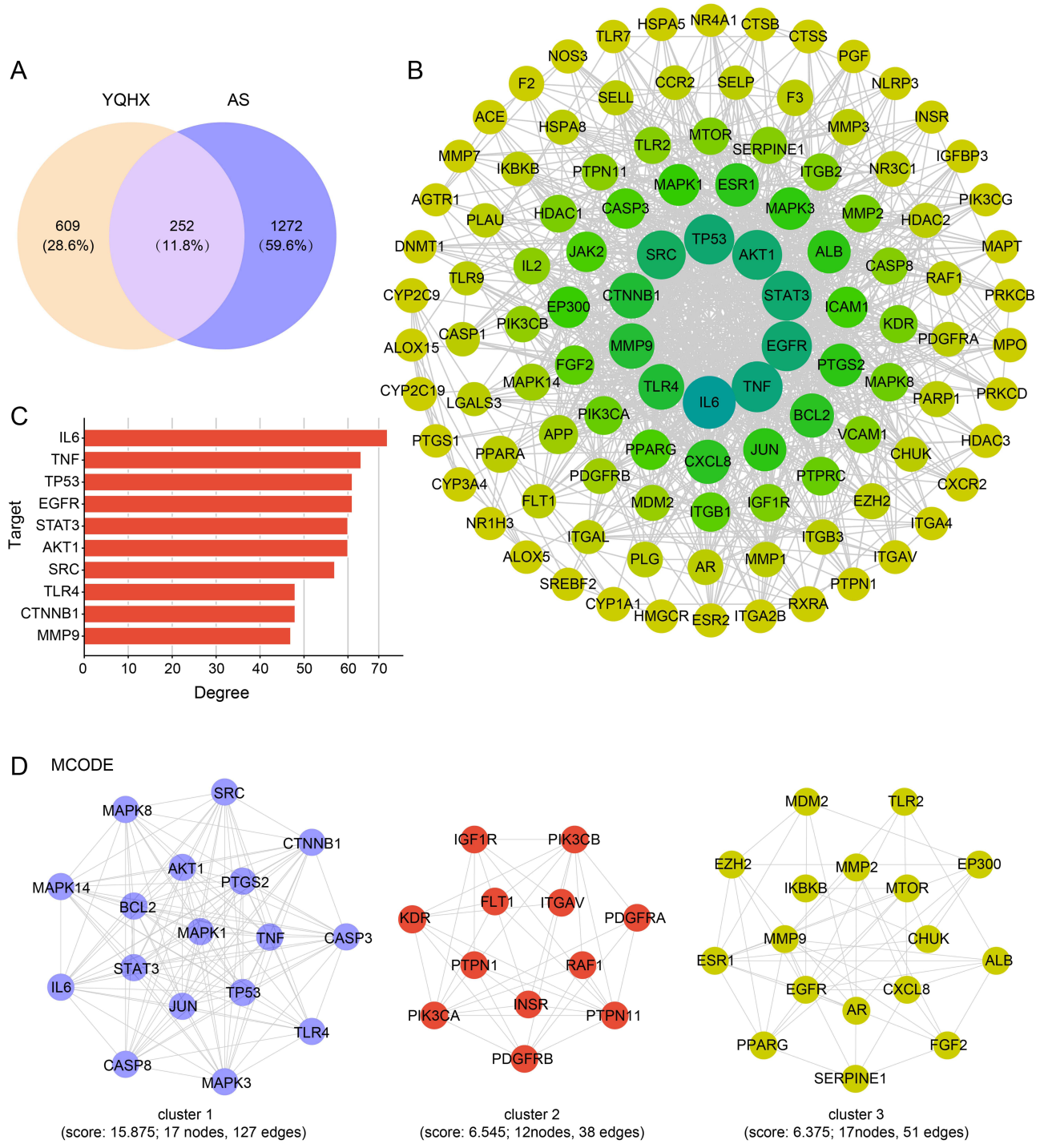

Figure 2 PPI analysis of the therapeutic targets of YQHX against AS. (**A**) Venn diagram illustrating the overlap between YQHX-related targets and AS-related targets. (**B**) PPI network of the overlapping therapeutic targets. (**C**) Bar graph illustrating the top 10 hub targets ranked by degree centrality. (**D**) Significant modules identified from the PPI network utilizing the MCODE algorithm, indicating three representative subnetworks (clusters 1–3).

(Figure 2B), numerous key targets demonstrated high node degrees and central placement, highlighting their potential significance in the therapeutic efficacy of YQHX. Figure 2C illustrates the top 10 hub nodes—IL-6, TNF, EGFR, TP53, AKT, STAT3, SRC, CTNNB1, TLR4, and MMP-9.—ranked by degree centrality, along with their respective values.

Key modules within the network were identified utilizing the Molecular Complex Detection (MCODE) plug-in: cluster 1 comprised 17 genes, cluster 2 encompassed 12 genes, and cluster 3 included 17 genes (Figure 2D). These three

https://doi.org/10.2147/JIR.S566368

subnetworks underwent additional examination through gene ontology biological process (GO-BP) enrichment analysis. Cluster 1 was enriched in 97 biological processes, including "positive regulation of apoptotic process" and "positive regulation of gene expression." Cluster 2 was enriched in 33 processes, including the "insulin receptor signaling pathway" and "insulin-like growth factor receptor signaling pathway." Cluster 3 was enriched in 21 biological processes, encompassing "positive regulation of gene expression" and "positive regulation of transcription by RNA polymerase II."

Construction of Compound-Target Network

A comprehensive compound–target network was initially established (Supplementary Figure S2). It comprised 423 nodes (36 active compounds and 252 targets) and 1,102 edges. In this comprehensive network, compounds of identical chemical class are organized within individual boxes; prenol lipids and glycerophospholipids represent the largest classes and engage with the highest number of target proteins, indicating their pivotal roles in facilitating the therapeutic effects of YQHX against AS. The compound nodes with the highest quercetin 3-gentiobioside (YQHX31, degree 50), purine (YQHX25, 47), kojic acid (YQHX4, 45), PC (16:0/16:0) (YQHX20, 45), galactosamine (YQHX2, 44), gallic acid methyl ester (YQHX29, 44), ginsenoside Rb1 (YQHX11, 42), ginsenoside Rb2 (YQHX12, 41), PC (O-18:1/20:4) (YQHX22, 41), and PC (18:1/18:2) (YQHX19, 40) exhibited the highest degrees. The top-ranking targets in the comprehensive network included PTGS2 (degree 19), ADORA2A (18), MMP2 (15), MMP13 (15), HSD11B1 (15), MMP9 (14), KDR (14), PTGS1 (14), CYP19A1 (14), and PTPN1 (14), indicating that these proteins may serve as critical hubs in the multi-target profile of YQHX.

A simplified core network was extracted to enhance visualization and emphasize mechanistically relevant interactions, as presented in Figure 3. This core network comprises 12 representative compounds—quercetin 3-gentiobioside, purine, kojic acid, galactosamine, ginsenoside Rb1, ginsenoside Rb2, PC(16:0/16:0), PC(18:1/18:2), PC(O-18:1/20:4), albiflorin, spiraeoside, and calceolarioside A—and 11 key targets, including PTGS2, ADORA2A, MMP2, MMP9, KDR, SRC, AKT1, EGFR, IL-6, TNF, and STAT3. In this simplified network, compound nodes were labeled with their chemical names, and the robust connectivity between these bioavailable constituents and hub proteins highlights them as central components of the target network that facilitates the anti-atherosclerotic action of YQHX.

Enrichment Analysis

The mechanisms of YQHX in treating AS were further clarified through GO and KEGG enrichment analyses. Figure 4A illustrates the top 10 GO terms, including biological processes (BP), molecular functions (MF), and cellular components (CC), which exhibit significant enrichment in inflammation-related categories, including "inflammatory response" and "response to lipopolysaccharide." These findings indicate the involvement of anti-inflammatory mechanisms in the therapeutic benefits of YQHX. Figure 4B depicts the top 25 KEGG pathways, highlighting notable enrichment in essential signaling pathways including "Lipid and atherosclerosis," "PI3K-Akt signaling pathway," and "MAPK signaling pathway." These pathways were further classified into four major functional domains: environmental information processing, cellular processes, organismal systems, and human diseases (Figure 4C). The predominantly enriched pathways were associated with human diseases, highlighting the clinical significance of the identified targets.

Results of Molecular Docking

According to the network pharmacology findings, ten active compounds and ten central protein targets were selected for molecular docking analysis. The protein targets were determined as the top 10 hub nodes ranked by degree value in the PPI network, while the selection of active compounds was based on a combined evaluation of their drug-likeness properties according to Lipinski's Rule of Five and their connectivity with these hub targets within the compound–target network. A binding energy of ≤ -5.0 kcal/mol is generally considered indicative of strong molecular affinity. Figure 5A depicts the heatmap of binding affinities. EGFR, AKT1, and SRC exhibited low binding energies, indicating strong docking activity and stable interactions between these proteins and the active compounds. These proteins may represent key targets through which YQHX manifests its therapeutic actions. Figure 5B illustrates six representative docking patterns between target proteins and their respective active compounds.

 https://doi.org/10.2147/JIR.S566368

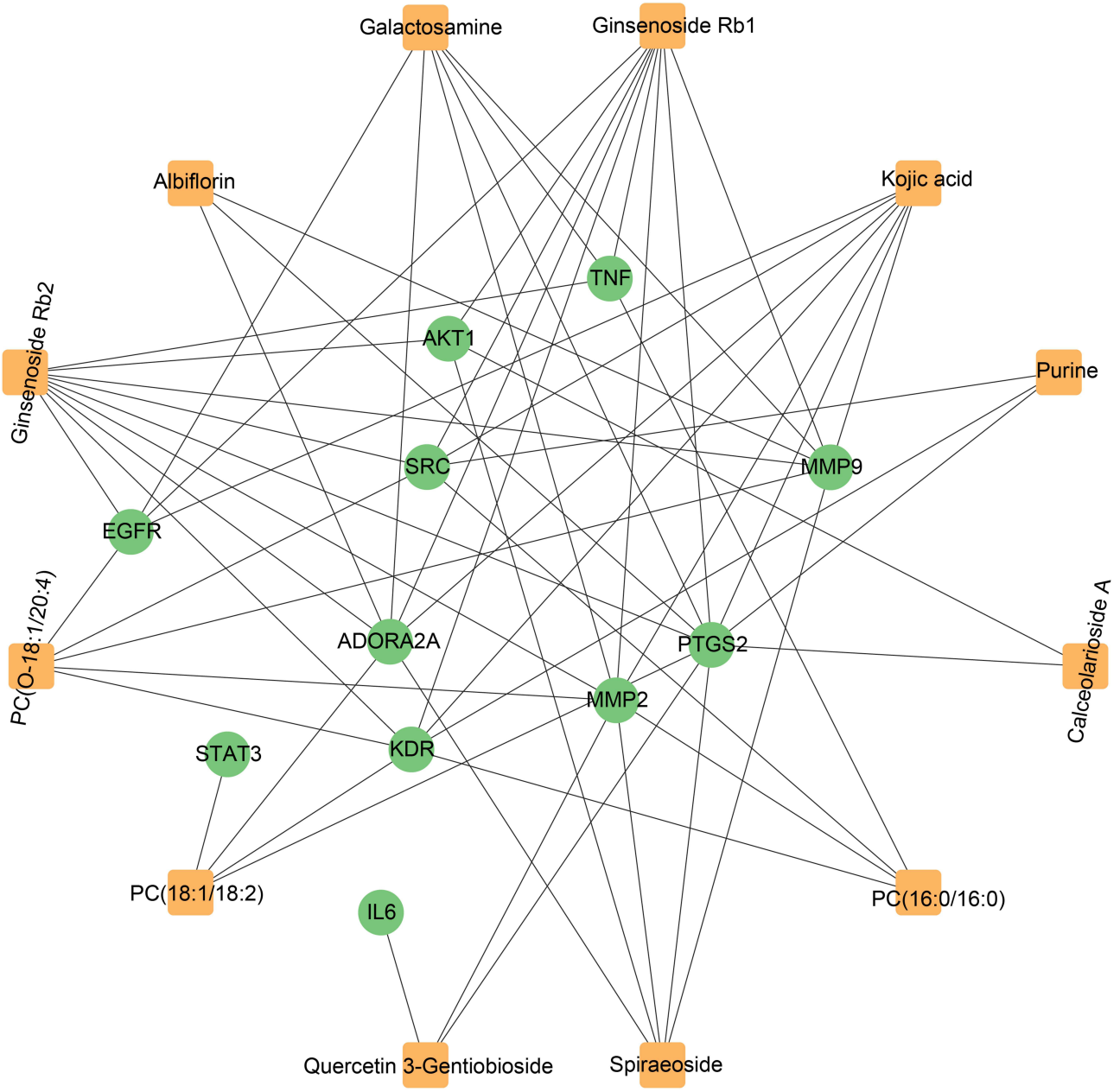

Figure 3 Simplified core compound–target network of YQHX against AS. This figure indicates a simplified network comprising 12 representative bioavailable compounds and 11 key targets extracted from the full compound–target network (Supplementary Figure S2). Compound nodes are indicated as circles and labeled with their chemical names, target nodes as squares, and edges indicate predicted interactions between compounds and targets.

YQHX Relieves Aortic Plaques in ApoE$^{-/-}$ Mice

To investigate the inhibitory effects of YQHX on AS, ApoE$^{-/-}$ mice fed an HFD were employed as the model. As illustrated in Figures 6A–C, the model group exhibited extensive atherosclerotic lesions compared to the control group, with significantly increased plaque area in the whole aorta and aortic root (model versus control: $P < 0.001$ for each) and significantly enhanced lipid deposition within aortic root plaques (model versus control: $P < 0.001$). Compared with the model group, the low- and high-dose YQHX groups (YQHX-L, YQHX-H) and the RST group exhibited significant reductions in atherosclerotic plaque area in the whole aorta and aortic root (YQHX-L versus model: $P = 0.0018$ for whole aorta, $P < 0.001$ for aortic root; YQHX-H versus model: $P < 0.001$ for both whole aorta and aortic root; RST versus model: $P < 0.001$ for both whole aorta and aortic root). Additionally, ORO staining of the aortic root demonstrated that

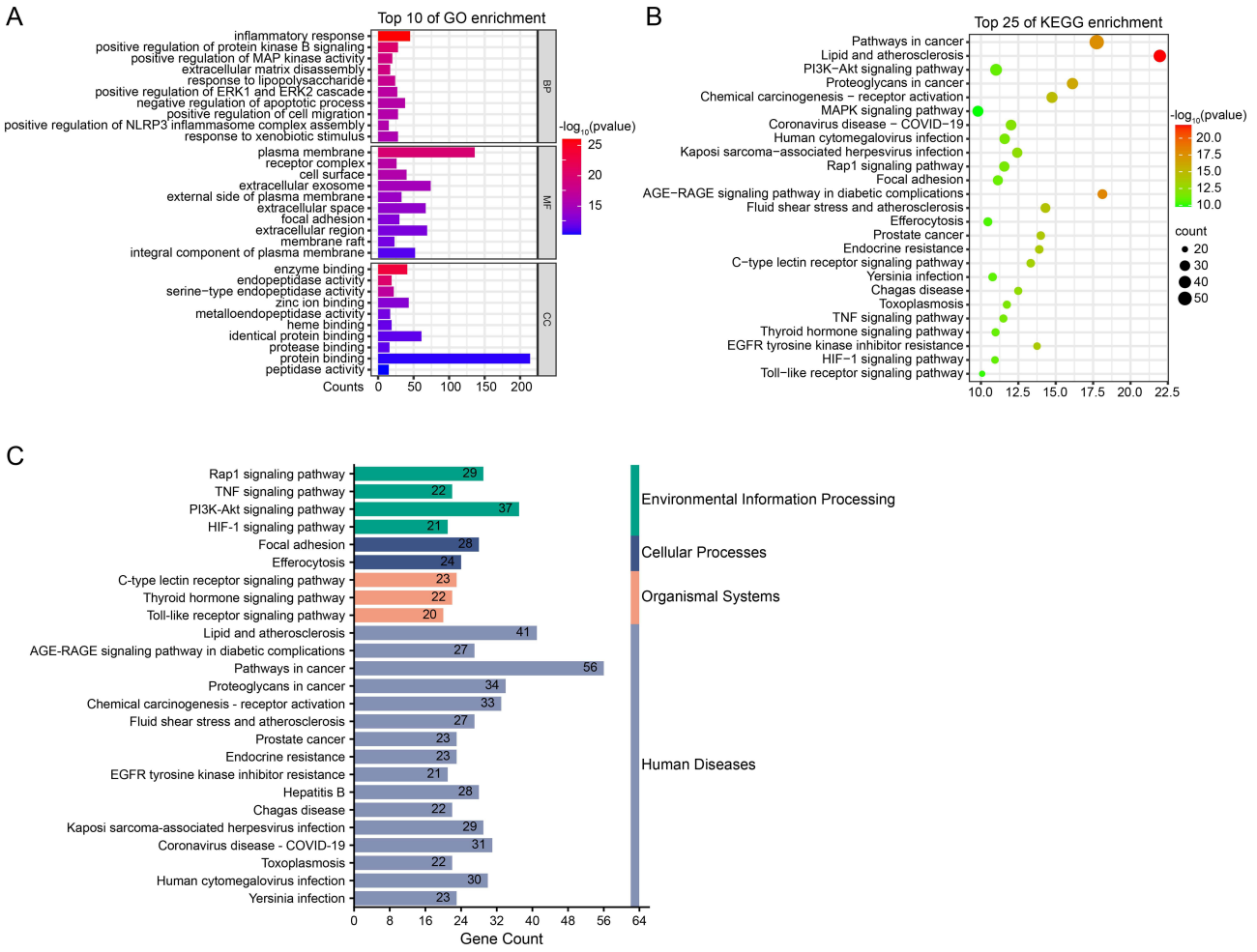

Figure 4 Predicted mechanisms of YQHX in the treatment of AS. (**A**) GO enrichment analysis of BP, MF, and CC. (**B**) KEGG pathway enrichment analysis (**C**) Functional classification of the top 25 KEGG-enriched pathways based on KEGG taxonomic analysis.

YQHX-L, YQHX-H, and RST exhibited significantly decreased lipid deposition within plaques (YQHX-L versus model: $P = 0.0115$; YQHX-H versus model: $P = 0.0068$; RST versus model: $P = 0.0108$). These findings indicate that low and high doses of YQHX effectively attenuate atherosclerotic plaque progression in vivo.

YQHX Ameliorates Lipid Metabolism Disorder in ApoE$^{-/-}$ Mice

Lipid metabolic dysregulation is recognized as a crucial factor in AS pathogenesis. To evaluate the effects of YQHX on blood lipid profiles, ApoE$^{-/-}$ mice fed an HFD were treated with YQHX-L, YQHX-H, or RST. As illustrated in Figures 7A–C, the model group exhibited markedly increased serum cholesterol (TC), triglyceride (TG), and low-density lipoprotein (LDL-C) levels compared with the control group (model versus control, $P < 0.001$ for each), whereas HDL-C levels were significantly decreased in the model group compared with the control group (Figure 7D, model versus control, $P < 0.001$). Compared with the model group, YQHX-L, YQHX-H, and RST significantly reduced TC, TG, and LDL-C levels (all treatment groups versus model, $P < 0.001$ for each), whereas no significant changes were observed in HDL-C among the treatment groups (Figure 7D). ORO staining of liver tissues consistently demonstrated significant lipid droplet accumulation in the model group compared to the control group (Figure 7E, model versus control, $P < 0.001$), whereas hepatic lipid accumulation was significantly diminished in the YQHX-L, YQHX-H, and RST groups (YQHX-L versus model, $P = 0.01$; YQHX-H versus model, $P = 0.012$; RST versus model, $P = 0.008$). Collectively, these findings indicate that low and high doses of YQHX exert beneficial effects in ameliorating lipid metabolic dysregulation in atherosclerotic mice.

https://doi.org/10.2147/JIR.S566368

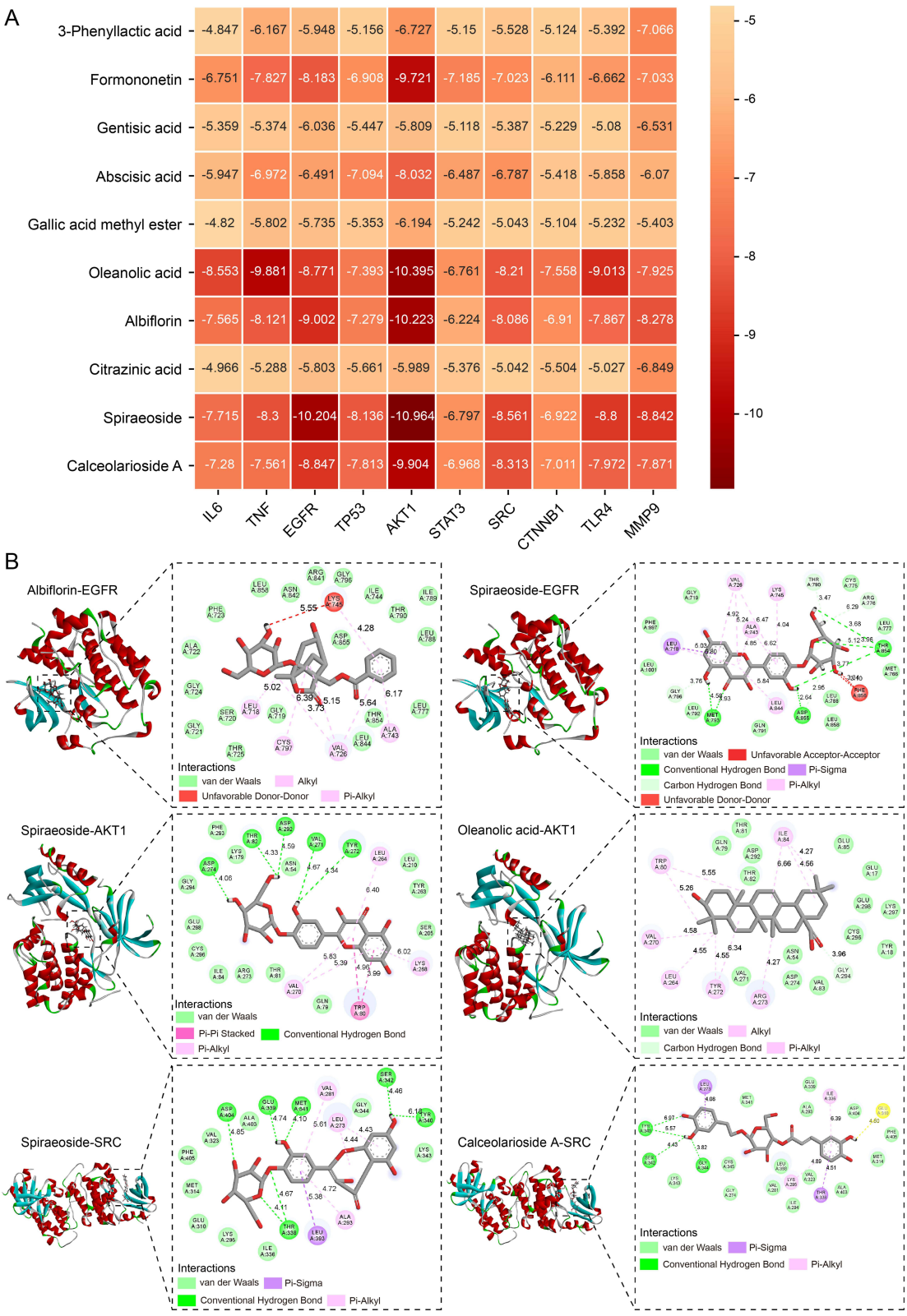

Figure 5 Binding energies and representative docking models. (**A**) Heatmap of binding affinities between active compounds and the ten hub protein targets. (**B**) Representative docking models for EGFR, AKT1, and SRC, illustrated in 3D and two-dimensional (2D) representations.

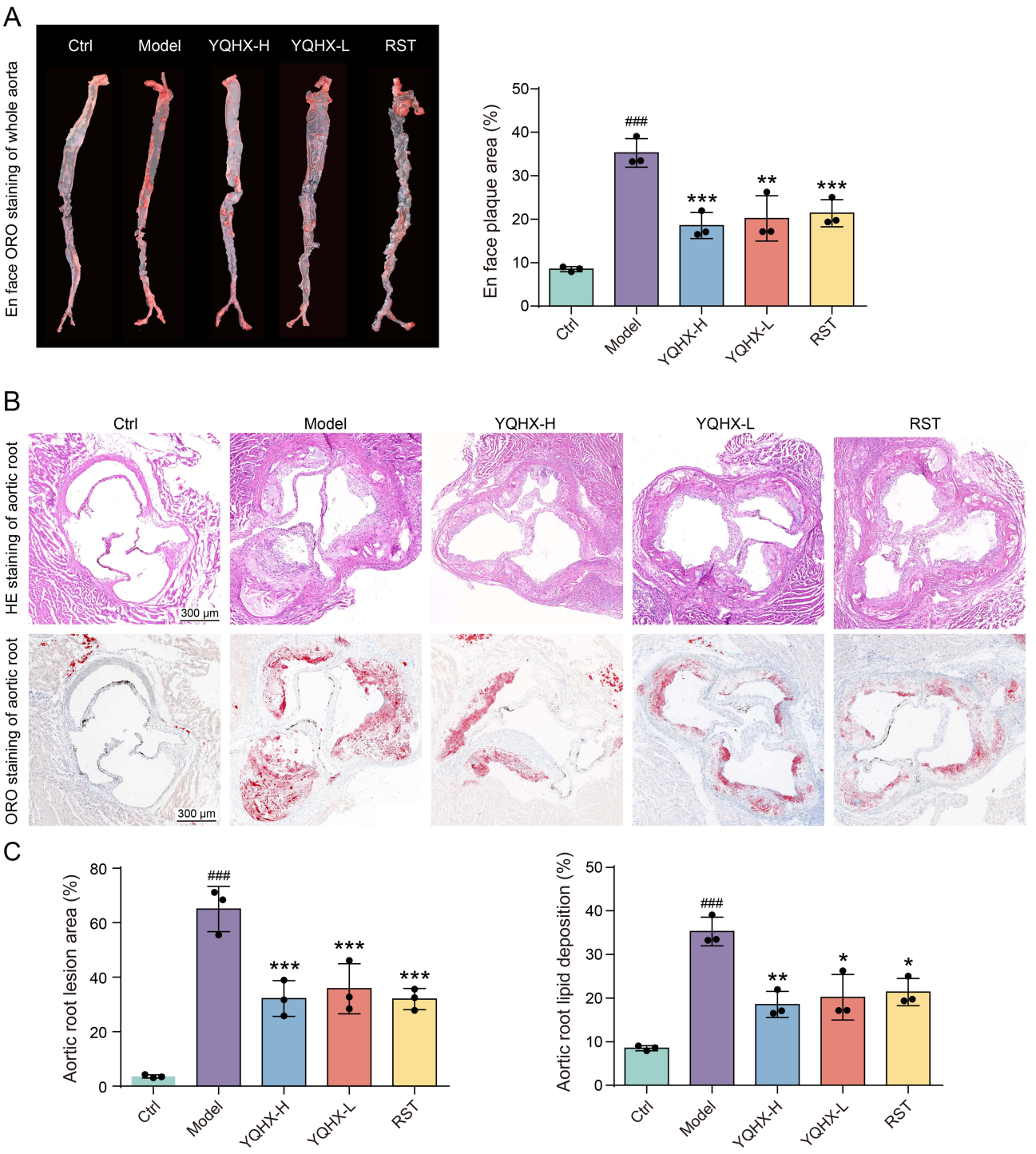

Figure 6 Effects of YQHX on aortic plaques in ApoE$^{-/-}$ mice. (**A**) ORO staining of en face aortas (n = 3). (**B**) Representative HE and ORO staining images of the aortic root sections (n = 3). (**C**) Quantification of lesion area (HE) and lipid-rich area (ORO) in aortic root sections. Data are expressed as means ± SD. $^{###}P < 0.001$ versus control, $^{*}P < 0.05$ versus model, $^{**}P < 0.01$ versus model, $^{***}P < 0.001$ versus model.

YQHX Inhibits the Inflammatory Response in ApoE$^{-/-}$ Mice

Given the crucial role of inflammation in AS and the findings from enrichment analysis, we further assessed the effect of YQHX on inflammatory responses in HFD-fed ApoE$^{-/-}$ mice. The model group exhibited significantly elevated serum levels of IL-6, IL-1β, sVCAM-1, and TNF-α compared to the control group (Figures 8A–D; model versus control, $P < 0.001$ for each), confirming the successful induction of a systemic inflammatory state. Compared with the model group, YQHX-L,

https://doi.org/10.2147/JIR.S566368

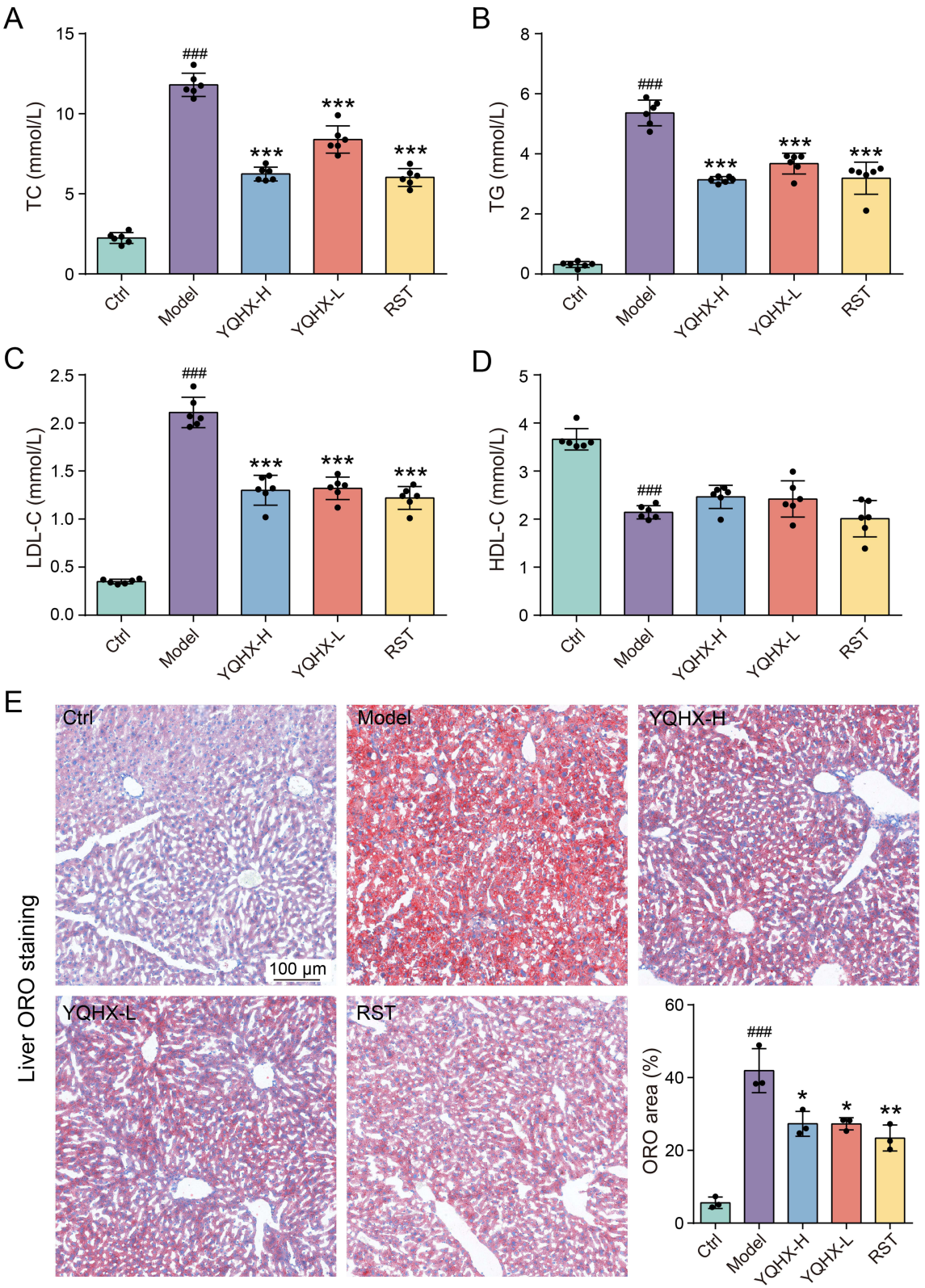

Figure 7 Effects of YQHX on blood lipid profiles and hepatic lipid accumulation in ApoE$^{-/-}$ mice. (**A–D**) Serum concentrations of TC, TG, LDL-C, and HDL-C in mice (n = 6). (**E**) Oil Red O (ORO) staining of frozen liver sections in mice (n = 3). Data are expressed as means ± SD. $^{###}P < 0.001$ versus control, $^{*}P < 0.05$ versus model, $^{**}P < 0.01$ versus model, $^{***}P < 0.001$ versus model.

https://doi.org/10.2147/JIR.S566368

YQHX-H, and RST significantly decreased serum IL-6, IL-1β, and sVCAM-1, whereas no significant differences were observed in TNF-α among the treatment groups (Figures 8A–D; IL-6: YQHX-L versus model, $P = 0.005$; YQHX-H versus model, $P = 0.023$; RST versus model, $P = 0.478$; IL-1β: all treatment groups versus model, $P < 0.001$ for each; sVCAM-1:

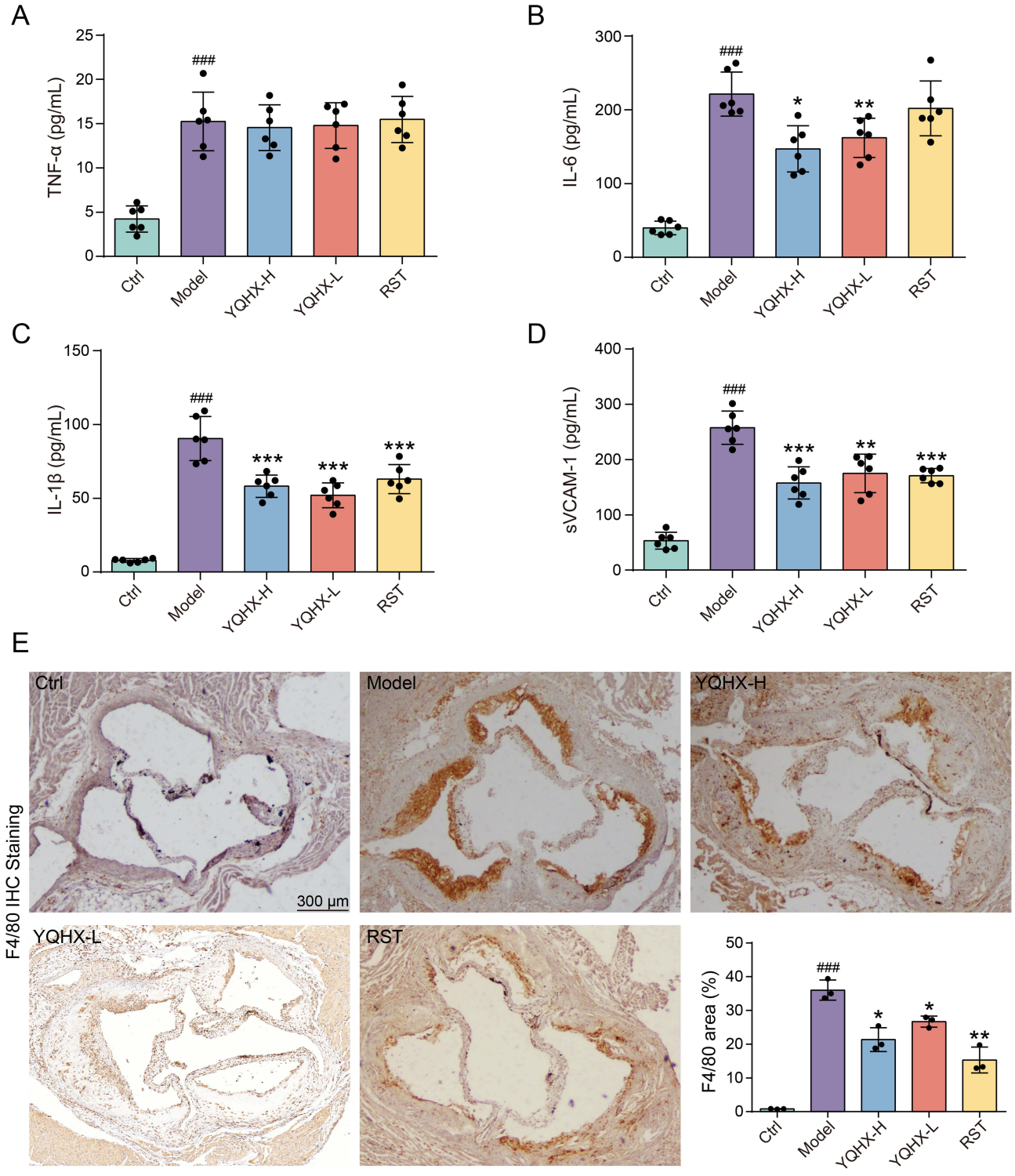

Figure 8 Effects of YQHX on serum inflammatory cytokines and macrophage infiltration within atherosclerotic plaques in ApoE$^{-/-}$ mice. (**A–D**) Concentrations of TNF-α, IL-6, IL-1β, and sVCAM-1 in serum (n = 6). (**E**) Immunohistochemistry staining of F4/80 in plaques (n = 3). Data are expressed as means ± SD. $^{###}P < 0.001$ versus control, $^{*}P < 0.05$ versus model, $^{**}P < 0.01$ versus model, $^{***}P < 0.001$ versus model.

https://doi.org/10.2147/JIR.S566368

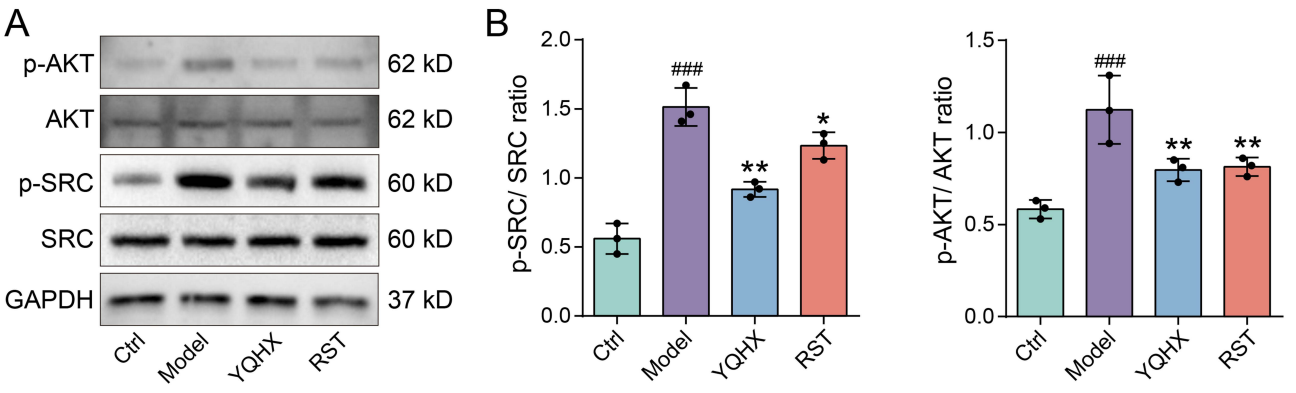

Figure 9 Effects of YQHX on SRC and AKT phosphorylation in atherosclerotic plaques of ApoE$^{-/-}$ mice. (**A**) Representative Western blotting images illustrating phosphorylated and total SRC and AKT expression in aortic plaque regions. (**B**) Quantitative analysis of the relative phosphorylation levels of SRC and AKT (n = 3). Data are expressed as means ± SD. $^{\#\#\#}P < 0.001$ versus control, $^{*}P < 0.05$ versus model, $^{**}P < 0.01$ versus model.

YQHX-L versus model, $P = 0.0013$; YQHX-H versus model, $P < 0.001$; RST versus model, $P < 0.001$). Consistently, IHC staining revealed that F4/80 expression within atherosclerotic plaques in the aortic root was significantly increased in the model group compared with the control group (Figure 8E, model versus control, $P < 0.001$), whereas YQHX-L, YQHX-H, and RST significantly reduced F4/80-positive area relative to the model group (YQHX-L versus model, $P = 0.038$; YQHX-H versus model, $P = 0.01$; RST versus model, $P = 0.003$), indicating reduced macrophage infiltration. These findings demonstrate that low and high doses of YQHX exert potent anti-inflammatory effects in this AS model.

Effect of YQHX on the Key Targets

Phosphorylation levels of key targets SRC and AKT in aortic plaque regions were evaluated using Western blotting. The findings indicated that phosphorylation levels of SRC and AKT were significantly upregulated in the model group compared to the control group, whereas YQHX (high dose) treatment effectively inhibited these changes (Figures 9A and B; p-SRC: model versus control, $P < 0.001$; YQHX versus model, $P = 0.002$; RST versus model, $P = 0.038$; p-AKT: model versus control, $P < 0.001$; YQHX versus model, $P = 0.003$; RST versus Model, $P = 0.004$). These findings indicated that YQHX could ameliorate atherosclerotic plaque progression through inhibition of the SRC/AKT signaling pathway.

Discussion

This study combined serum pharmacochemistry, network pharmacology, molecular docking, and in vivo validation to systematically uncover the multi-component and multi-target pathways through which YQHX exerts anti-atherosclerotic effects. We identified 36 absorbed constituents in YQHX-containing serum. Network pharmacology analysis of 252 overlapping YQHX–AS targets revealed inflammation and lipid metabolism as key functional themes and identified SRC and AKT as pivotal nodes. These predictions were confirmed in ApoE$^{-/-}$ mice, where YQHX significantly attenuated aortic plaque burden, enhanced lipid profiles, diminished systemic and plaque inflammation, and inhibited SRC/AKT phosphorylation within lesions. Collectively, our findings offer mechanistic evidence for the conventional application of YQHX in atherosclerotic diseases and position the SRC/AKT axis as an essential molecular hub through which this formula restores vascular homeostasis. Similar integrated strategies that merge network pharmacology with experimental validation have been utilized for other traditional formulations for cardiovascular diseases, generally highlighting MAPK, NF-κB, or STAT3-related pathway.[30,31] However, few studies have integrated serum pharmacochemistry-based identification of bioavailable constituents with a convergent focus on SRC/AKT signaling in AS, marking a significant innovation of the current study.

Serum pharmacochemistry revealed that YQHX introduces a relatively restricted but structurally varied array of 36 bioavailable compounds into the bloodstream, with prenol lipids being the predominant subclass. Upon mapping to the compound–target network, prenol lipids and glycerophospholipids exhibited the highest connectivity to protein targets, indicating that these lipophilic components may function as primary mediators of YQHX's in vivo activity. Ginsenosides and oleanolic acid possess anti-inflammatory, antioxidant, endothelial-protective, and lipid metabolism-modulating

properties, which collectively mitigate atherosclerotic progression.[32,33] Albiflorin, a compound found in *Paeoniae Rubra Radix*, reduces cytoplasmic lipid deposition and inhibits foam cell formation through the LOX-1/NF-κB signaling pathway.[34] Furthermore, an animal study demonstrated that kaempferol, a bioactive compound present in *Carthami Flos, Astragali Radix*, and *Ginseng Radix et Rhizoma*, effectively inhibited HFD-induced AS in rabbits by regulating the expression of inflammation-related markers.[35] Collectively, our observations substantiate the notion that YQHX functions through a constellation of serum-available components that collectively interact with multiple targets implicated in lipid-driven vascular inflammation.

The PPI network offered a comprehensive perspective of how these targets may cooperate in AS. Among the 252 overlapping targets, conventional inflammatory mediators (IL-6, TNF, TLR4, and STAT3), growth factor receptors (EGFR), kinases (AKT1 and SRC), and matrix-remodeling enzymes (MMP-9) were identified as hub nodes based on degree centrality. This topology suggests that YQHX is positioned to affect upstream cytokine signaling and downstream effector mechanisms, including extracellular matrix remodeling and endothelial barrier control. MCODE analysis further decomposed the PPI network into densely interconnected clusters, each enriched in specific biological processes.[36] One cluster was enriched in inflammatory and apoptotic regulation, another in insulin and insulin-like growth factor receptor signaling, and a third in transcriptional regulation. These modules indicate that YQHX may simultaneously regulate inflammatory pathways, metabolic signaling, and gene expression programs that converge on AS progression. This network design is highly consistent with the current understanding of AS as a chronic lipid-mediated inflammatory disease, wherein intertwined inflammatory and metabolic pathways facilitate endothelial dysfunction, plaque growth, and destabilization.[37,38]

GO and KEGG enrichment analyses more functional background for these interacting targets. The enriched GO terms notably encompassed "inflammatory response" and "response to lipopolysaccharide," implicating innate immune activation and endotoxin-related signaling in the therapeutic context of YQHX. KEGG analysis revealed that "lipid and atherosclerosis," "PI3K–Akt signaling pathway," and "MAPK signaling pathway" are among the top pathways, predominantly classified into human disease-related modules. These findings align with clinical and experimental evidence that chronic interaction between lipid accumulation and vascular inflammation drives AS,[39] with PI3K–Akt and MAPK cascades serving as key integrators of dyslipidemia and inflammatory responses in the vessel wall.[40,41] In this context, our data indicate that YQHX may function by rebalancing the lipid–inflammation axis through coordinated control of PI3K–Akt and related signaling networks.

In this network context, SRC and AKT1 have emerged as notable, compelling targets. Both proteins ranked among the top hub nodes and resided at the intersection of inflammation-related and metabolism-related pathways. SRC, a non-receptor tyrosine kinase, modulates endothelial barrier integrity and leukocyte transmigration through the phosphorylation of junctional proteins,[42] whereas AKT assimilates upstream receptor signals to regulate lipid metabolism, cellular survival, and NF-κB–dependent inflammatory responses.[43,44] Previous studies of AS and other cardiovascular diseases have primarily focused on PI3K–Akt signaling downstream of growth factor receptors or pattern recognition receptors,[40,45] and numerous herbal formulations have been reported to act, at least in part, through modulation of this pathway.[46,47]

Molecular docking offered structural-level validation for prioritizing EGFR, AKT1, and SRC as principal targets of YQHX-derived constituents. For EGFR, albiflorin was accommodated in a hydrophobic subpocket and established multiple alkyl contacts with Leu718, Val726, Ala743, and Cys797, indicating a contact arrangement of its non-polar framework within the binding cleft. Furthermore, an additional alkyl contact involving Lys745 was associated with an unfavorable donor–donor interaction, indicating a minor local steric/electrostatic disadvantage. However, spiraeoside formed a more comprehensive interaction network with EGFR: it engaged Leu718 through π–σ and π–alkyl interactions and contacted Leu844, Lys745, Ala743, and Val726 via π–alkyl contacts, and formed conventional hydrogen bonds with Met793, Thr854, and Asp855; only an adverse acceptor–acceptor interaction with Phe856 was observed. Spiraeoside also docked favorably to AKT1 and SRC. In the AKT1 complex, it formed conventional hydrogen bonds with Asp274, Tyr272, Val271, Asp292, and Thr82, whereas its aromatic rings engaged Trp80 through π–π stacking and contacted Val270, Lys268, and Leu264 via π–alkyl interactions, collectively creating a robust hydrogen-bonding and hydrophobic network consistent with stable occupancy of the ATP-binding site. Oleanolic acid, a triterpenoid component, interacted with AKT1 almost exclusively through hydrophobic interaction, forming alkyl interactions with Trp80, Val270, Leu264, Tyr272, Arg273, and Ile84, in line with deep insertion of its lipophilic backbone into a non-polar pocket. In SRC, spiraeoside formed conventional hydrogen bonds with Asp404, Thr338, Tyr340, Ser342, Met341, and Glu339, complemented by π–σ and π–alkyl interactions with Leu393, Ala293, and

Leu273, whereas calceolarioside A formed a similar pattern of conventional hydrogen bonds with Tyr340, Ser342, and Gly344 and π–σ/π–alkyl contacts with Lys295, Thr338, Ile336, and Leu273. Similar docking-based analyses have been employed to predict interactions between herbal constituents and cardiovascular targets.[48] Collectively with the favorable docking scores, the synergistic hydrogen-bonding and hydrophobic/π interaction profiles suggest that multiple representative constituents of YQHX can directly and stably interact with EGFR, AKT1, and SRC, thereby offering structural plausibility for the modulation of SRC/AKT-centered signaling as predicted by network analysis and validated in vivo.

In vivo experiments in ApoE$^{-/-}$ mice offered essential biological validation of the multi-layered in silico predictions, indicating that YQHX significantly diminished atherosclerotic plaque burden in the whole aorta and aortic root, with concomitant reduction in plaque lipid deposition and hepatic lipid accumulation. These structural advantages were coupled with enhanced systemic lipid profiles—evidenced by significant decreases in TC, TG, and LDL-C without affecting HDL-C—indicating that YQHX primarily exerts athero-protection by decreasing atherogenic lipoproteins and restricting plaque lipid accumulation rather than elevating HDL-C levels. Although increased HDL-C levels have been observed in ApoE$^{-/-}$ mice under specific experimental conditions,[49] other investigations have indicated that HDL-C remains stable or diminished.[50,51] Therefore, HDL-C behavior in this model appears context-dependent. In our experimental setting, HDL-C exhibited a significant decline in the model group relative to the control group, whereas YQHX did not induce a statistically significant restoration of HDL-C compared with the model group, potentially reflecting variations in dietary composition, intervention duration, or strain background compared with previous studies, and does not negate a robust anti-atherosclerotic effect primarily attributed to reductions in TC, TG, and LDL-C. Consistent with the enrichment of inflammation-related GO and KEGG terms, YQHX exhibited significant anti-inflammatory activity, significantly reducing serum IL-6, IL-1β, and sVCAM-1 levels and decreasing macrophage accumulation in aortic root plaques. However, TNF-α levels remained unchanged, suggesting that IL-6/IL-1β–centered pathways may constitute the primary inflammatory mechanism targeted by this formulation. These simultaneous lipid-lowering and anti-inflammatory effects are consistent with the current view that correction of dyslipidemia and attenuation of vascular inflammation are key determinants of plaque stabilization and cardiovascular risk reduction in AS.[52] Notably, Western blotting revealed that YQHX markedly inhibited SRC and AKT phosphorylation within plaques, reversing the elevated p-SRC and p-AKT levels observed in untreated AS mice and directly correlating the network- and docking-based predictions to functional pathway modulation in vivo. Collectively, these findings support a model wherein YQHX lowers atherogenic lipids, mitigates systemic and intraplaque inflammation, and fortifies the endothelial-inflammatory microenvironment by inhibiting SRC/AKT signaling.

These findings also contextualize YQHX among other Qi-invigorating and blood-activating formulations used in AS treatment. Maijitong granule (MJT), which contains several core components similar to YQHX (*Astragali Radix, Salvia miltiorrhiza Bunge, and Paeoniae Rubra Radix*), attenuates atherosclerosis in LDLR$^{-/-}$ mice by simultaneously reducing plaque burden, enhancing plaque stability, suppressing inflammatory cytokines, inhibiting foam cell formation, and, critically, limiting ferroptosis through STAT6 activation and subsequent suppression of DMT1- and SOCS1/p53-dependent lipid peroxidation and iron dysregulation.[53] QiShenYiQi pill (QSYQ), another traditional Qi-invigorating formulation, mitigates aortic lesions in ApoE$^{-/-}$ mice primarily by enhancing reverse cholesterol transport, marked by downregulation of CD36 and upregulation of the PPARγ–LXRα/β–ABCA1 axis, alongside extensive transcriptional reprogramming of lipid metabolic pathways.[54] Conversely, our study emphasizes the SRC/AKT axis as a central signaling hub for YQHX: YQHX enhances systemic lipid profiles and reduces plaque lipid deposition and suppresses IL-6/IL-1β/sVCAM-1 and macrophage infiltration and directly inhibits SRC and AKT phosphorylation within plaques. Accordingly, although MJT and QSYQ have been mechanistically conceptualized primarily based on ferroptosis inhibition and cholesterol efflux–mediated lipid clearance, YQHX seems to operate at a more proximal signaling level by modulating SRC/AKT-centered pathways that integrate endothelial barrier integrity with inflammatory and metabolic signaling. This indicates that YQHX may be especially appropriate for AS phenotypes characterized by endothelial dysfunction and intraplaque inflammation, offering a mechanistic enhancement to current Qi-invigorating formulations that primarily target ferroptosis or reverse cholesterol transport.

This study has some limitations. First, although the inhibition of SRC/AKT phosphorylation within plaques provided strong support for the involvement of this axis, it remains correlative: more definitive evidence of causality would require

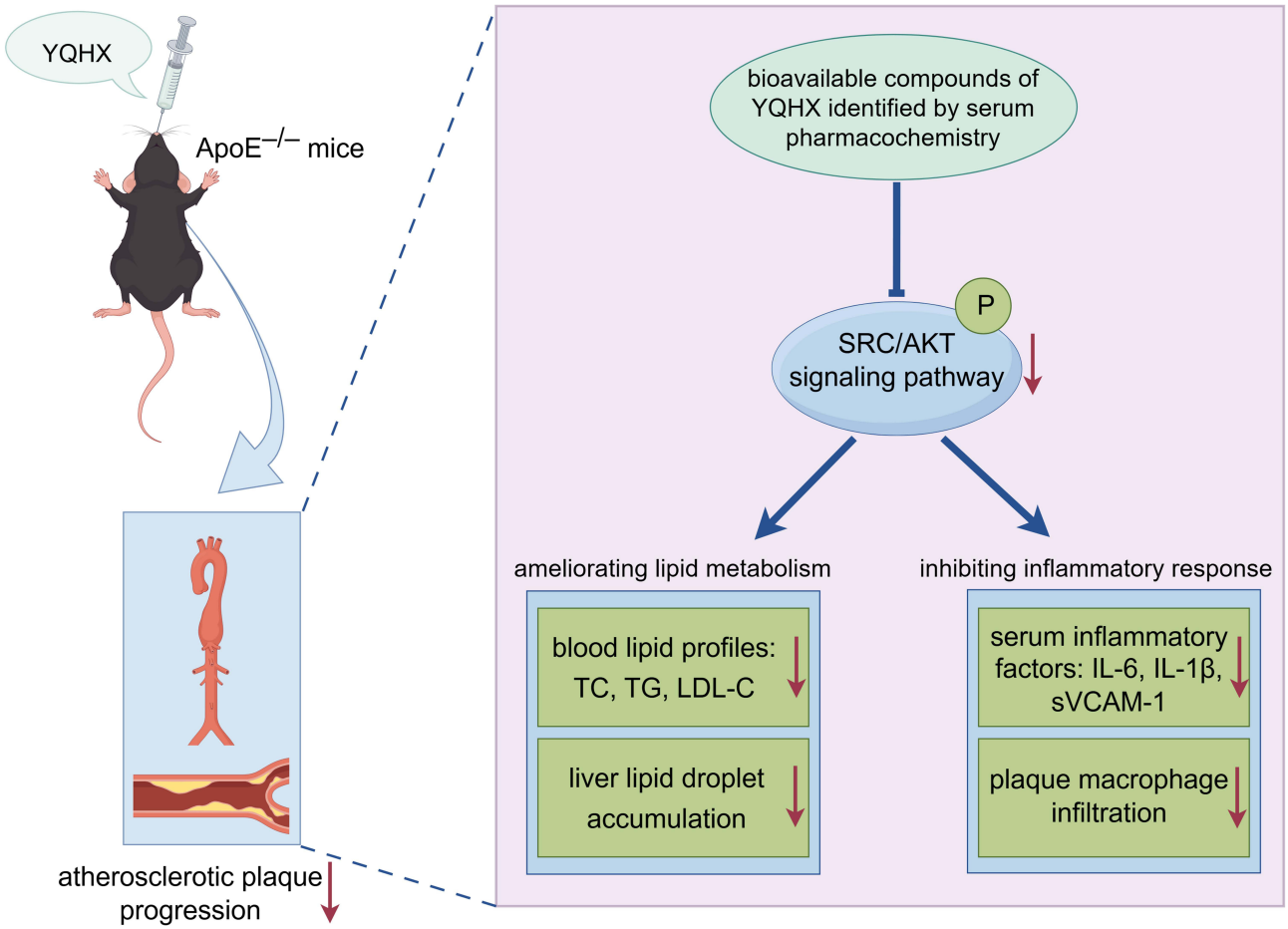

Figure 10 Integrated mechanistic diagram of YQHX against AS. Schematic overview of the proposed mechanism by which YQHX-derived bioavailable compounds inhibit the SRC/AKT signaling axis, thereby improving lipid metabolism and attenuating vascular inflammation, ultimately leading to a reduced atherosclerotic plaque burden in ApoE$^{-/-}$ mice.

gain- and loss-of-function approaches, including pharmacological inhibition or overactivation of SRC/AKT to test whether these interventions replicate or mitigate the effects of YQHX, which is beyond the scope of this study and represents a logical next step. Second, other hub targets identified herein (IL-6, TLR4, STAT3, and MMPs) were not mechanistically analyzed in the animal tissues and may also influence the comprehensive therapeutic profile of YQHX. Future work will incorporate targeted molecular analyses to elucidate their specific roles in mediating the effects of YQHX. Third, although two dose levels of YQHX were included, the overall biological effects of the two doses were largely comparable, and the absence of an additional dose gradient limits the ability to fully evaluate dose dependency; expanding dose–response assessment will therefore be an important priority in subsequent studies. To elucidate our current findings despite these limitations, we have synthesized the proposed multi-component, multi-target, and multi-pathway actions of YQHX into an integrated mechanistic diagram (Figure 10), which may function as a framework for future mechanistic and translational investigations.

Conclusion

This study systematically identified the serum-absorbed active compounds of YQHX and revealed its multi-targeted therapeutic mechanisms against AS. Utilizing UPLC-Q-Exactive Orbitrap-MS detection, network pharmacology, molecular docking, and in vivo validation in ApoE$^{-/-}$ mice, we established that YQHX mitigates atherosclerotic plaque formation by regulating lipid metabolism and inhibiting inflammatory responses. Mechanistically, YQHX exerts anti-atherosclerotic effects at least in part through the inhibition of the SRC/AKT signaling pathway. These findings offer a scientific basis for the clinical

https://doi.org/10.2147/JIR.S566368

application of YQHX in atherosclerotic cardiovascular diseases and present novel insights into the pharmacological actions of TCM formulations regarding lipid-induced chronic inflammation.

Abbreviations

AS, atherosclerosis; YQHX, Yiqi Huoxue granule; TCM, traditional Chinese medicine; ApoE$^{-/-}$, apolipoprotein E knockout; Ox-LDL, oxidized low-density lipoprotein; MMPs, matrix metalloproteinases; LPS, lipopolysaccharide; UHPLC, ultra-high-performance liquid chromatography; AGC, automatic gain control; KEGG, Kyoto Encyclopedia of Genes and Genomes; GO, Gene ontology; SRC, proto-oncogene tyrosine-protein kinase Src; AKT, Protein kinase B; HRP, horseradish peroxidase; ELISA, enzyme-linked immunosorbent assay; SD, standard deviation; ANOVA, one-way analysis of variance; MCODE, Molecular Complex Detection; BP, biological process; MF, molecular functions; CC, cellular components; HDF, high-fat diet; RST, rosuvastatin; ORO, oil red O; HE, hematoxylin-eosin; IHC, immunohistochemistry; DAB, diaminobenzidine; PPI, protein-protein interactions; TNF-α, tumor necrosis factor-alpha; IL-6, interleukin-6; IL-1β, interleukin-1 beta; sVCAM-1, soluble vascular cell adhesion molecule-1; TC, total cholesterol; TG, triglycerides; LDL-C, low-density lipoprotein cholesterol; HDL-C, high-density lipoprotein cholesterol.

Data Sharing Statement

The datasets used and/or analysed during the current study are available from the corresponding author on reasonable request.

Ethics Statement

All animal experiments were conducted following the ARRIVE guidelines (https://arriveguidelines.org/arrive-guidelines) and approved by the Medical Ethical Committee of Henan Province Hospital of Traditional Chinese Medicine (Zhengzhou, China, approval number: PZ-HNSZYY-2022-035).

Author Contributions

Xinzhou Wang: Investigation, Methodology, Software, Visualization, Writing – original draft, Writing – review & editing. Shanshan Liu: Investigation, Software, Visualization, Writing – original draft, Writing – review & editing. Zehao Lei: Investigation, Methodology, Writing – original draft. Panxia Cao: Investigation, Software, Visualization, Writing – original draft. Weili Shi: Formal Analysis, Writing – review & editing. Shuibo Gao: Formal Analysis, Writing – review & editing. Hong Wu: Methodology, Formal Analysis, Funding acquisition, Project administration, Writing – review & editing. All authors reviewed and approved the final version of the paper. All authors have agreed on the journal to which the article has been submitted; and agree to be accountable for all aspects of the work.

Funding

This work was supported by grants from the Henan Provincial Natural Science Foundation (Grant No. 232300420054) and the Henan Provincial Science and Technology Research Project (Grant No. 242102310447 and No. 242102311208).

Disclosure

The authors declare that they have no competing interests.

References

1. Kobiyama K, Ley K. Atherosclerosis. *Circ Res*. 2018;123(10):1118–1120. doi:10.1161/CIRCRESAHA.118.313816
2. Ruiz-Leon AM, Lapuente M, Estruch R, Casas R. Clinical advances in immunonutrition and atherosclerosis: a review. *Front Immunol*. 2019;10:837. doi:10.3389/fimmu.2019.00837
3. Tsao CW, Aday AW, Almarzooq ZI, et al. Heart disease and stroke statistics-2023 update: a report from the American Heart Association. *Circulation*. 2023;147(8):e93–e621. doi:10.1161/CIR.0000000000001123
4. Hansson GK. Inflammation, atherosclerosis, and coronary artery disease. *N Engl J Med*. 2005;352(16):1685–1695. doi:10.1056/NEJMra043430
5. Geovanini GR, Libby P. Atherosclerosis and inflammation: overview and updates. *Clin Sci*. 2018;132(12):1243–1252. doi:10.1042/CS20180306
6. Kong P, Cui ZY, Huang XF, Zhang DD, Guo RJ, Han M. Inflammation and atherosclerosis: signaling pathways and therapeutic intervention. *Signal Transduct Target Ther*. 2022;7(1):131. doi:10.1038/s41392-022-00955-7

7. Jebari-Benslaiman S, Galicia-Garcia U, Larrea-Sebal A, et al. Pathophysiology of Atherosclerosis. *Int J Mol Sci*. 2022;23(6):3346. doi:10.3390/ijms23063346
8. Jiang H, Zhou Y, Nabavi SM, et al. Mechanisms of oxidized LDL-mediated endothelial dysfunction and its consequences for the development of atherosclerosis. *Front Cardiovasc Med*. 2022;9:925923. doi:10.3389/fcvm.2022.925923
9. Moore KJ, Sheedy FJ, Fisher EA. Macrophages in atherosclerosis: a dynamic balance. *Nat Rev Immunol*. 2013;13(10):709–721. doi:10.1038/nri3520
10. Olejarz W, Lacheta D, Kubiak-Tomaszewska G. Matrix metalloproteinases as biomarkers of atherosclerotic plaque instability. *Int J Mol Sci*. 2020;21(11):3946. doi:10.3390/ijms21113946
11. Zhang W, Lv S, Zhu Y, Zhang J. Current advances in syndromology of qi deficiency and blood stasis syndrome in coronary heart disease: a critical review. *J Tradit Chin Med*. 2021;62(12):1092–1096.
12. Wang X, Gao S, Dai L, Wang Z, Han L, Wu H. Effect of Yiqi Huoxue formula on inflammation and endothelial injury induced by lipopolysaccharide in mice. *Chin J Integr Tradit West Med*. 2020;40(07):823–828.
13. Wu H, Wang X, Gao S, et al. Effect of yiqi huoxue formula on inflammation induced by lipopolysaccharide in endothelial cells. *Chin J Integr Tradit West Med*. 2019;39(02):200–205.
14. Tang YP, Xu DQ, Yue SJ, Chen YY, Fu RJ, Bai X. Modern research thoughts and methods on bio-active components of TCM formulae. *Chin J Nat Med*. 2022;20(7):481–493. doi:10.1016/S1875-5364(22)60206-1
15. Yu Y, Yao C, Guo DA. Insight into chemical basis of traditional Chinese medicine based on the state-of-the-art techniques of liquid chromatography-mass spectrometry. *Acta Pharm Sin B*. 2021;11(6):1469–1492. doi:10.1016/j.apsb.2021.02.017
16. Zhao L, Zhang H, Li N, et al. Network pharmacology, a promising approach to reveal the pharmacology mechanism of Chinese medicine formula. *J Ethnopharmacol*. 2023;309:116306. doi:10.1016/j.jep.2023.116306
17. Noonan J, Cardoso L, Bobik A, Peter K. Atherosclerotic plaque instability and rupture: recommended mouse models to empower clinically relevant discoveries, diagnostics, and therapeutics. *Arterioscler Thromb Vasc Biol*. 2025;45(10):1707–1714. doi:10.1161/ATVBAHA.125.321011
18. Wu H, Gao H, Gao S, et al. A Chinese 4-herb formula, Yiqi-Huoxue granule, alleviates H(2)O(2)-induced apoptosis by upregulating uncoupling protein 2 in H9c2 cells. *Phytomedicine*. 2019;53:171–181. doi:10.1016/j.phymed.2018.09.031
19. Daina A, Michielin O, Zoete V. SwissTargetPrediction: updated data and new features for efficient prediction of protein targets of small molecules. *Nucleic Acids Res*. 2019;47(W1):W357–W364. doi:10.1093/nar/gkz382
20. Stelzer G, Rosen N, Plaschkes I, et al. The genecards suite: from gene data mining to disease genome sequence analyses. *Curr Protoc Bioinformatics*. 2016;54:1.30.1–33. doi:10.1002/cpbi.5
21. Wishart DS, Feunang YD, Guo AC, et al. DrugBank 5.0: a major update to the DrugBank database for 2018. *Nucleic Acids Res*. 2018;46(D1):D1074–D1082. doi:10.1093/nar/gkx1037
22. Amberger JS, Hamosh A. Searching online mendelian inheritance in man (OMIM): a knowledgebase of human genes and genetic phenotypes. *Curr Protoc Bioinformatics*. 58:1.2.1–12. doi:10.1002/cpbi.27
23. Barbarino JM, Whirl-Carrillo M, Altman RB, Klein TE. PharmGKB: a worldwide resource for pharmacogenomic information. *Wiley Interdiscip Rev Syst Biol Med*. 2018;10(4):e1417. doi:10.1002/wsbm.1417
24. Szklarczyk D, Gable AL, Lyon D, et al. STRING v11: protein-protein association networks with increased coverage, supporting functional discovery in genome-wide experimental datasets. *Nucleic Acids Res*. 2019;47(D1):D607–D613. doi:10.1093/nar/gky1131
25. Sherman BT, Hao M, Qiu J, et al. DAVID: a web server for functional enrichment analysis and functional annotation of gene lists (2021 update). *Nucleic Acids Res*. 2022;50(W1):W216–W221. doi:10.1093/nar/gkac194
26. Shannon P, Markiel A, Ozier O, et al. Cytoscape: a software environment for integrated models of biomolecular interaction networks. *Genome Res*. 2003;13(11):2498–2504. doi:10.1101/gr.1239303
27. Morris GM, Huey R, Olson AJ. Using AutoDock for ligand-receptor docking. *Curr Protoc Bioinformatics*. 2008;Chapter 8. doi:10.1002/0471250953.bi0814s24.
28. Burley SK, Berman HM, Kleywegt GJ, Markley JL, Nakamura H, Velankar S. Protein Data Bank (PDB): the single global macromolecular structure archive. *Methods Mol Biol*. 2017;1607:627–641. doi:10.1007/978-1-4939-7000-1_26
29. Wang Y, Bryant SH, Cheng T, et al. PubChem BioAssay: 2017 update. *Nucleic Acids Res*. 2017;45(D1):D955–D963. doi:10.1093/nar/gkw1118
30. Li D, Chen R, Xu X, et al. Integrated metabolomics and network pharmacology to reveal the mechanisms of Shexiang Baoxin pill against atherosclerosis. *Phytomedicine*. 2024;135:156138. doi:10.1016/j.phymed.2024.156138
31. Zhang Y, Qi Y, Jia Z, et al. Effects and mechanisms of Zhizi Chuanxiong herb pair against atherosclerosis: an integration of network pharmacology, molecular docking, and experimental validation. *Chin Med*. 2024;19(1):8. doi:10.1186/s13020-023-00874-x
32. Xue Q, He N, Wang Z, et al. Functional roles and mechanisms of ginsenosides from Panax ginseng in atherosclerosis. *J Ginseng Res*. 2021;45(1):22–31. doi:10.1016/j.jgr.2020.07.002
33. Jannus F, Sainz J, Reyes-Zurita FJ. Principal bioactive properties of oleanolic acid, its derivatives, and analogues. *Molecules*. 2024;29(14):3291. doi:10.3390/molecules29143291
34. Sun J, Li X, Jiao K, Zhai Z, Sun D. Albiflorin inhibits the formation of THP-1-derived foam cells through the LOX-1/NF-kappaB pathway. *Minerva Med*. 2019;110(2):107–114. doi:10.23736/S0026-4806.18.05711-7
35. Kong L, Luo C, Li X, Zhou Y, He H. The anti-inflammatory effect of kaempferol on early atherosclerosis in high cholesterol fed rabbits. *Lipids Health Dis*. 2013;12:115. doi:10.1186/1476-511X-12-115
36. Bader GD, Hogue CW. An automated method for finding molecular complexes in large protein interaction networks. *BMC Bioinf*. 2003;4:2. doi:10.1186/1471-2105-4-2
37. Ruan Q, Guan P, Qi W, et al. Porphyromonas gingivalis regulates atherosclerosis through an immune pathway. *Front Immunol*. 2023;14:1103592. doi:10.3389/fimmu.2023.1103592
38. Shi L, Du X, Li J, Zhang G. Bioinformatics and systems biology approach to identify the pathogenetic link between psoriasis and cardiovascular disease. *Clin Cosmet Invest Dermatol*. 2023;16:2283–2295. doi:10.2147/CCID.S421193
39. Birukov KG. Oxidized lipids: the two faces of vascular inflammation. *Curr Atheroscler Rep*. 2006;8(3):223–231. doi:10.1007/s11883-006-0077-x
40. Zhang Y, Han L, Wang Y, Wang M. The Role of the PI3K/Akt/mTOR pathway in atherosclerosis: mechanisms, therapeutic potential, and emerging targeted treatments. *Curr Atheroscler Rep*. 2025;27(1):115. doi:10.1007/s11883-025-01364-1

41. Ajoolabady A, Pratico D, Lin L, et al. Inflammation in atherosclerosis: pathophysiology and mechanisms. *Cell Death Dis*. 2024;15(11):817. doi:10.1038/s41419-024-07166-8
42. Chatterjee V, Yang X, Ma Y, et al. Endothelial microvesicles carrying Src-rich cargo impair adherens junction integrity and cytoskeleton homeostasis. *Cardiovasc Res*. 2020;116(8):1525–1538. doi:10.1093/cvr/cvz238
43. Gao F, Sabbineni H, Artham S, Somanath PR. Modulation of long-term endothelial-barrier integrity is conditional to the cross-talk between Akt and Src signaling. *J Cell Physiol*. 2017;232(10):2599–2609. doi:10.1002/jcp.25791
44. Cong X, Kong W. Endothelial tight junctions and their regulatory signaling pathways in vascular homeostasis and disease. *Cell Signal*. 2020;66:109485. doi:10.1016/j.cellsig.2019.109485
45. Qin W, Cao L, Massey IY. Role of PI3K/Akt signaling pathway in cardiac fibrosis. *Mol Cell Biochem*. 2021;476(11):4045–4059. doi:10.1007/s11010-021-04219-w
46. Liu X, Liu L, Ren X, et al. Unveiling XinJia-LuHuang Granules' protective mechanism against atherosclerosis: integrating network pharmacology, metabolomics, and experimental validation. *Phytomedicine*. 2025;143:156919. doi:10.1016/j.phymed.2025.156919
47. Shi Y, Zhang Y, Cai Y, et al. Key proteins identification of Buyang Huanwu Decoction in regulating macrophage polarization to alleviate atherosclerosis via an integrated strategy combining network pharmacology, batch molecular docking and experimental verification. *Int J Biol Macromol*. 2025;310(Pt 3):143380. doi:10.1016/j.ijbiomac.2025.143380
48. Ding Y, Xiang Q, Zhu P, et al. Qihuang Zhuyu formula alleviates coronary microthrombosis by inhibiting PI3K/Akt/alphaIIbbeta3-mediated platelet activation. *Phytomedicine*. 2024;125:155276. doi:10.1016/j.phymed.2023.155276
49. Feng X, Du M, Li S, et al. Hydroxysafflor yellow A regulates lymphangiogenesis and inflammation via the inhibition of PI3K on regulating AKT/mTOR and NF-kappaB pathway in macrophages to reduce atherosclerosis in ApoE-/- mice. *Phytomedicine*. 2023;112:154684. doi:10.1016/j.phymed.2023.154684
50. Zhang Y, Gu Y, Chen Y, et al. Dingxin Recipe IV attenuates atherosclerosis by regulating lipid metabolism through LXR-alpha/SREBP1 pathway and modulating the gut microbiota in ApoE(-/-) mice fed with HFD. *J Ethnopharmacol*. 2021;266:113436. doi:10.1016/j.jep.2020.113436
51. Qiu R, Long J, Zhou L, et al. Yangyin qingre huoxue method in traditional chinese medicine ameliorates atherosclerosis in apoE(-/-) Mice suffering from high-fat diet and HSP65 aggression. *Evid Based Complement Alternat Med*. 2019;2019:2531979. doi:10.1155/2019/2531979
52. Libby P. The changing landscape of atherosclerosis. *Nature*. 2021;592(7855):524–533. doi:10.1038/s41586-021-03392-8
53. Shi J, Yang MM, Yang S, et al. MaiJiTong granule attenuates atherosclerosis by reducing ferroptosis via activating STAT6-mediated inhibition of DMT1 and SOCS1/p53 pathways in LDLR(-/-) mice. *Phytomedicine*. 2024;128:155489. doi:10.1016/j.phymed.2024.155489
54. Xie J, Peng L, Wang T, et al. QiShenYiQi pill inhibits atherosclerosis by promoting reverse cholesterol transport PPARgamma-LXRalpha/beta-ABCA1 pathway. *J Ethnopharmacol*. 2023;315:116684. doi:10.1016/j.jep.2023.116684